CLM-R 103

CLM-R 103

United Kingdom Atomic Energy Authority
RESEARCH GROUP

Report

RADIATION DAMAGE EFFECTS IN THE CONTAINMENT VESSEL OF A THERMONUCLEAR REACTOR

D. G. MARTIN

Culham Laboratory
Abingdon Berkshire

1970

Available from H. M. Stationery Office
EIGHT SHILLINGS NET

C.18

U.D.C.
621.039.63 : 539.12.04

RADIATION DAMAGE EFFECTS IN THE CONTAINMENT VESSEL OF A THERMONUCLEAR REACTOR

by

D.G. Martin

(Metallurgy Division, A.E.R.E., Harwell)

ABSTRACT

During the lifetime of a thermonuclear reactor the containment vessel, assumed here to be fabricated from niobium, will be irradiated by about 2×10^{23} of 14·1 MeV neutrons cm^{-2}. This will result in high concentrations of transmutation products (for example 10 atomic per cent of zirconium) and an appreciable number of displacements of the atoms.

A detailed discussion is given of the physical property changes due to this radiation damage for irradiation temperatures in the range 600-1200°C.

Helium is expected to be the most serious transmutation product since it can aggregate into comparatively immobile bubbles and so produce swelling of the containment vessel. Assuming bubbles are maintained in equilibrium it is shown that swelling under conditions anticipated in the reactor should not be too excessive (~ a few per cent) for irradiation temperatures up to about 1000°C; also that below this temperature fracture under tensile stresses due to the growth of bubbles is not expected in practice.

Displacement damage may harden the material, enhance its creep rate and result in swelling due to void formation. An attempt is made to predict the importance of these effects from the point of view of a reactor designer. Swelling due to voids could well be important since void formation is predicted within the temperature range 600-1100°C.

Erosion of the vessel and contamination of the plasma due to the evaporation of niobium atoms from thermal spikes located near the surface is shown to be unimportant.

A number of experiments using currently available irradiation sources, which could shed further light on this subject, are suggested and discussed.

U.K.A.E.A. Research Group,
Culham Laboratory,
Abingdon,
Berkshire

March, 1970

CONTENTS

LIST OF TABLE CAPTIONS

1. INTRODUCTION

If a significant amount of power in this country is to be generated by means of fusion reactors it will be necessary to show that

(a) satisfactory plasma containment parameters can be achieved,

(b) the engineering problems associated with the construction and running of a fusion reactor can be solved, and

(c) power from a thermonuclear reactor is at least no more expensive than that from more conventional sources of power.

In the past the containment problem has received most attention. However, it is recognised that much work will have to be done before the engineering problems have been answered satisfactorily. Naturally these three items are inter-related, as is evident from two recent economic evaluations of fusion power[1,2]; these reports indicate that economic power is feasible provided that the overall power from a reactor is sufficiently high (about 5000 MW(th) in ref.1 and 10,000 MW(e) in ref.2). In the present report we shall be concerned with one of the engineering problems, namely the effect of the irradiation due to neutrons produced in the reactor on the integrity of the containment vessel; however some of the assumptions made in this feasibility study, such as the neutron flux and operating temperature, will be based on economics, which in their turn are connected with containment considerations.

The purpose of the present report is to consider in detail the various radiation damage effects in the containment vessel and to predict as far as possible the accompanying physical property changes. No attempt is made to relate these changes with the design considerations for specific reactor systems. In many cases it is inevitable that at present these predictions can only be tentative; as a result some possible experiments are suggested which might improve this situation.

Many of the conclusions arrived at here have already been reported briefly in paper 4.5 presented at the Culham Conference on Nuclear Fusion Reactors, 17-19 September, 1969.

2. FORMULATION OF THE PROBLEM

2.1 Some Basic Assumptions

We shall assume that all fusions of nuclei in the reactor occur by the reaction

$$H^2 + H^3 = (He^4 + 3{\cdot}5\ \text{MeV}) + (n + 14{\cdot}1\ \text{MeV}) \qquad \ldots (1)$$

where the brackets indicate the distribution between the resulting particles of the 17.6 MeV of energy released. In the present study we shall ignore completely the readiation

damage due to the α particles produced by this reaction since it will be assumed that the magnetic fields prevent them from reaching the walls. We are thus concerned with the radiation damage produced in the containment vessel as the 14·1 MeV neutrons escape from the plasma. For the sake of simplicity we shall assume that each neutron passes through the wall only once, i.e. that there is no backscattering of neutrons by the material surrounding the wall.

Following Carruthers et al[1] we shall assume that the containment vessel of the reactor is in the form of a toroid with minor and major radii of 175 and 550 cm respectively. so that the wall area is $3{\cdot}80 \times 10^6$ cm^2. For the sake of simplicity we suppose that 22·2 MeV is liberated as a result of each fusion event, namely 17·6 MeV from fusion, Equation (1), plus 4·6 MeV from the $Li^6(n,T)\alpha$ reaction used to breed tritium. Although this figure is only approximate since it ignores other nuclear reactions, in particular the (n,2n) reactions, it should be sufficiently accurate for our present purposes. Hence for a 5000 MW reactor, which will be assumed to operate at a constant power output rate, $1{\cdot}4 \times 10^{21}$ neutrons are formed per second, corresponding to a flux of $3{\cdot}7 \times 10^{14}$ neutrons cm^{-2} sec^{-1} incident on the wall. This implies that the overall dose the containment vessel will have to withstand during the life-time of the reactor, assumed to be 20 years, is $2{\cdot}3 \times 10^{23}$ neutrons cm^{-2}.

It appears that refractory metals are the most suitable materials out of which to fabricate the containment vessel. Thus Homeyer[3] suggested molybdenum and more recently Rose[2] favoured niobium. In the present work only niobium will be considered; however in view of the similarity in many of their properties a number of the conclusions arrived at here will be applicable as well to other refractory metals.

In their conceptual reactor systems Homeyer[3] and Fraas (see appendix of Rose[2]) suggest that the vacuum wall should run at about 600 and 1000°C respectively. As a result the present work spans the range 600-1200°C in an attempt to study the effect of temperature on the various radiation induced physical property changes.

2.2 The Interaction of 14·1 MeV Neutrons with Niobium

There are two types of interaction which need concern us here: (a) nuclear reactions and (b) collision processes which result in kinetic energy being imparted to specific niobium atoms.

2.2.1 Nuclear Transmutation Reactions

A large number of nuclear reactions occur between 14·1 MeV neutrons and Nb^{93} (100% natural abundance). The importance of these reactions is that impurities are

introduced into the material and so modify its physical properties.

The most important of these reactions are given below together with their cross sections σ[4], the decay schemes of the radioactive products, their half lives τ[5] and Q values[64].

$$\left\{ \begin{array}{l} Nb^{93} + n \longrightarrow Nb^{92} + 2n - 8{\cdot}8 \text{ MeV } (\sigma = 415 \pm 40 \text{ mbarn}) \quad \ldots (2a) \\ Nb^{92} \xrightarrow[\text{capture}]{\text{orbital electron}} Zr^{92} \ (\tau = 10{\cdot}1 \text{ days}) \quad \ldots (2b) \end{array} \right.$$

$$\left\{ \begin{array}{l} Nb^{93} + n \longrightarrow Y^{90} + \alpha + 4{\cdot}9 \text{ MeV } (\sigma = 9{\cdot}3 \pm {\cdot}5 \text{ mbarn}) \quad \ldots (3a) \\ \\ \qquad Y^{90} \xrightarrow[\beta^-]{} Zr^{90} \ (\tau = 64{\cdot}2 \text{ hour}) \end{array} \right.$$

$$\left\{ \begin{array}{l} Nb^{93} + n \longrightarrow Zr^{93} + p + 0{\cdot}7 \text{ MeV } (\sigma = 22 \pm 8 \text{ mbarn}) \quad \ldots (4a) \\ Zr^{93} \xrightarrow[\beta^-]{} Nb^{93} \ (\tau = 9{\cdot}5 \times 10^5 \text{ year}) \quad \ldots (4b) \end{array} \right.$$

$$Nb^{93} + n \longrightarrow Y^{89} + n + \alpha - 2{\cdot}0 \text{ MeV } (\sigma = 2{\cdot}5 \pm 1{\cdot}1 \text{ mbarn}) \quad \ldots (5)$$

We shall neglect the (n,2p) and (n,He^3) reactions since the corresponding cross-sections are less than 0·5 and 0·06 mbarn respectively; moreover no other chemical elements in addition to those formed by the reactions of Equations (2-5) are produced.

Combining those reactions which yield the same element the cross-sections for the production of each impurity is obtained and shown in Table 1. Also shown in the table is the concentration of each impurity produced by a dose of $2{\cdot}3 \times 10^{23}$ neutrons cm^{-2}.

TABLE 1

Cross sections for the production of impurities in niobium by 14·1 MeV neutrons and the atomic fractions formed in the reactor after 20 years.

	H	He	Y	Zr
Cross section (mbarn)	22 ± 8	$11{\cdot}8 \pm 1{\cdot}2$	$2{\cdot}5 \pm 1{\cdot}1$	446 ± 41
Atomic fraction	$5{\cdot}1 \pm 1{\cdot}9 \times 10^{-3}$	$2{\cdot}75 \pm {\cdot}28 \times 10^{-3}$	$5{\cdot}8 \pm 2{\cdot}6 \times 10^{-4}$	$\cdot 99 \pm \cdot 10 \times 10^{-1}$

For the purpose of evaluating the cross sections it was assumed that the reactions given by Equations (2b) and (3b) go to completion, while that given by Equation (4b) is so slow it may be ignored. A very precise calculation of these impurity concentrations is complicated because the various transmutation products can in their turn react with the fast

neutrons. However sufficiently accurate values are obtained by neglecting these secondary reactions, as was done here, since their cross sections are not particularly large (e.g. for Zr^{92}, the most abundant impurity, the (n,α) and (n,p) cross sections are about 10 and 22 mbarn respectively). As a result the concentrations of other impurity products formed by neutron interactions with the zironium and yttrium atoms are so small that they will be neglected.

In Section 3 the effect of these impurities on the properties of niobium is considered.

2.2.2 The Transfer of Kinetic Energy to Atoms

In discussing the various nuclear reactions which may occur we ignored the kinetic energy of the reaction products; this energy will subsequently be shared with other atoms of the solid. The magnitude of this energy is determined by the Q value of the reaction, the angles of emergence of the particles and the state of excitation of the heavier particle. In cases of interest here the energies of the light and heavy particles are of the order of 10 MeV and 100 keV respectively.

In addition, when the radioactive reaction products decay by the emission of particles or gamma rays the nuclei will recoil with an energy of the order of 10 keV in order to conserve momentum.

There are however two more important processes for transferring kinetic energy to atoms than those discussed above and which alone will be considered below, namely elastic and inalstic neutron scattering for which the corresponding cross sections are of the order of 1 barn. If elastic scattering between the incident neutron and a nucleus can be pictured as a simple billiard ball collision, then all energies imparted to the atom are equally probable up to a maximum energy T_{max} given by

$$T_{max} = \frac{4M}{(M+1)^2} E_n \qquad \ldots (6)$$

where E_n is the neutron energy and M the atomic weight of the target nucleus. When E_n = 14·1 MeV T_{max} = 594 keV in niobium. However in practice neutrons are scattered preferentially into the forward direction so that lower energy transfers are favoured, as discussed in Section 4.1. Inelastic scattering is a rather similar process except that the target nucleus is excited and decays subsequently by γ emission.

The way these energetic lattice atoms (often described in the literature as 'primary knockons') lose energy to the surrounding lattice has been discussed in detail by many authors in recent years. However for our present pruposes the earlier treatment by Kinchin and Pease[6] will suffice and may moreover be readily used in calculations.

When atoms possess energies greater than about A keV, where A is the atomic weight, most of the energy is dissipated by electronic excitation; this will leave the lattice structure of a metal unaffected and no physical property changes will ensue. On the other hand for energies lower than about A keV most of the energy is transferred by means of hard sphere collisions with the surrounding atoms. As a result the energy will be shared throughout the solid by means of a cascade process. However if an atom receives more than about 25 eV, denoted here by E_d, it will be displaced so that an interstitial atom and a vacant lattice site will be formed. Since it is these displaced atoms which modify the properties of the metal we need only concern ourselves with atoms in the cascade which receive an energy greater than E_d. If $E(< A$ keV) is the energy of an atom initiating a cascade the resulting number of atoms displaced will be $E/2E_d$. Clearly if E is greater than A keV the corresponding number of displaced atoms according to this model will be $A/2E_d$.

A more detailed account of the displacement of niobium atoms by 14·1 MeV neutrons, is given in Section 4.1.

3. THE EFFECT OF TRANSMUTATION PRODUCTS ON SOME PROPERTIES OF NIOBIUM

Two general types of transmutation product are formed (see Section 2.1): (a) solid impurities with atomic numbers close to that of niobium and (b) gaseous impurities with low atomic numbers. These are discussed in Sections 3.1 and 3.2 respectively.

3.1 Impurities Adjacent to Niobium in the Periodic Table

Table 1 shows that after 20 years $5{\cdot}8 \pm 2{\cdot}6 \times 10^{-4}$ atomic fraction of yttrium and $0{\cdot}99 \pm 0{\cdot}10 \times 10^{-1}$ of zirconium are formed. Although the yttrium-niobium system displays a very limited range of solubility[7] it is quite likely that such a small concentration will form a solid solution. However the data available at present is too meagre to be certain. The zirconium will be in solid solution since at 600°C and above the phase diagram indicates the occurrence of a single phase up to about 15 atomic % of zirconium[8].

The transmutation of an appreciable fraction of the niobium into zirconium could well improve the material's properties as a containment vessel. Thus between room temperature and 1000°C dilute alloys with zirconium possess a higher strength without an appreciable reduction in ductility; for example when pure niobium is converted into a 10% Zr alloy the yield strength rises from about 10,000 psi to 40,000 psi and the ductility falls from about 40% to 30% at 1095°C[9]. There is also evidence that the introduction of zirconium into niobium makes it more creep resistant (see ref.10 and Section 4.4).

Unfortunately the large fraction of niobium which is transmuted to zirconium in the reactor's lifetime means that the prediction of the other radiation effects is more complex. Indeed for the sake of simplicity we shall be compelled in general to neglect these transmutations in the subsequent discussion. However in any future experimental work designed to investigate radiation effects it will be possible to allow at least partially for transmutations by using dilute alloys with varying compositions of zirconium as a starting material.

3.2 Impurity Atoms of Low Atomic Number

It is evident from Equations (2-5) that three types of particles of low atomic number are produced by transmutation reactions, namely neutrons protons and alphas.

The neutrons may be neglected in this section since, to a high probability, their kinetic energy will enable them to escape from the containment wall. To a first approximation the (n,2n) reaction simply enhances the incident neutron flux; for example, with a 2 cm wall this enhancement factor is 4·6 ± 0·4 per cent. In the present report we shall ignore this factor since it will not modify our conclusions significantly. Note that under certain circumstances, for example when neutron economy calculations are being performed, allowance must be made for the fact that neutrons produced by (n,2n) and (n,nα) reactions will possess energies lower than 14·1 MeV.

The protons and alpha particles will lose their kinetic energy to the solid and become hydrogen and helium atoms, both of which are very insoluble impurities in niobium. Helium atoms will then diffuse and form aggregates which subsequently grow into bubbles. Most of the remainder of Section 3.2 will consider these bubbles and their effects on the physical properties of niobium.

In comparison the hydrogen atoms may be neglected in this section for two reasons. Firstly the diffusion coefficient is so high in the temperatures of interest here ($\sim 5 \times 10^{-4}$ cm^2 sec^{-1}[11]) that the instantaneous hydrogen atom concentration in the material is too low for appreciable aggregation and hence bubble formation to occur. Instead hydrogen atoms will diffuse to grain boundaries and then rapidly migrate along them to an external surface. This is further discussed in more quantitative terms in Section 3.2.2.1. Secondly the permeation rate is also very high ($\sim 10^2$ cc at N.T.P. per hour per cm^2 of surface at a temperature of 1000°C[12]). As a result hydrogen atoms which diffuse into helium bubbles will be able to permeate back into the solid in a comparatively short time and continue to diffuse to a grain boundary. We conclude therefore that to a good approximation all the hydrogen will escape through the inner and outer walls of the

containment vessel in a comparatively short time ($\approx$ 1 day) after being formed. Consequently the hydrogen will not affect the properties of the niobium.

3.2.1 The Effect of Helium Bubble Size on the Swelling of Niobium

Throughout the remainder of Section 3.2 we shall assume, following Table 1, that $2{\cdot}75 \times 10^{-3}$ atomic fraction of helium is present in the niobium. For the sake of simplicity we shall also assume in general that the helium is produced instantaneously and consider the subsequent behaviour of the niobium. This should result in no less drastic property changes compared with what actually occurs, namely the build-up of helium at a rate which is time independent and of magnitude such that the above concentation is attained after 20 years.

Let us suppose that this helium aggregates into a number of identical spherical bubbles randomly dispersed throughout the solid. Another basic assumption which is made here and is discussed in greater detail in Appendix 1 is that bubbles are always in equilibrium. The criterion for this is that

$$p = \frac{2\gamma}{r} \qquad \ldots (7)$$

where p is the gas pressure inside the bubble of radius r and with surface energy γ. Essentially the justification for this assumption is that the large concentration of mobile vacancies and interstitials produced by irradiation will assist the bubble radius to adjust itself to the equilibrium value since under these conditions strains in the surrounding lattice due to a bubble will vanish. Under these conditions the volume expansion of the solid is simply the volume contained in the gas bubbles.

If N is the number of helium atoms formed per cc of the solid, and n the number of helium atoms in each bubble then, assuming the perfect gas law

$$p\,\frac{4}{3}\,\pi r^3 = nkT \qquad \ldots (8)$$

to be valid, the fractional swelling Δ is given by

$$\Delta = \frac{rNkT}{2\gamma} \qquad \ldots (9)$$

However for small bubbles, when the pressure inside each bubble is large the perfect gas law is not valid. In Appendix 2 it is shown that for radii smaller than about 1000 Å a simplication of Van der Waals expression

$$p\left(\frac{4}{3}\pi r^3 - nb\right) = nkT \qquad \ldots (10)$$

may be used, when the swelling is

$$\Delta = N\left(\frac{rkT}{2\gamma} + b\right) \qquad \ldots (11)$$

Fig.1 shows the swelling as a function of bubble radius at 600, 1000 and 1200°C with the following constants assumed: γ = 2100 ergs cm^{-2}[13], N = $1{\cdot}50 \times 10^{20}$ helium atoms cm^{-3} (= $2{\cdot}75 \times 10^{-3}$ atomic fraction or 5·5 cc of helium gas at N.T.P. per cc of niobium), and b = $3{\cdot}937 \times 10^{-23}$ cc per atom[5]. This shows that the swelling increases considerably as the bubble radius increases. However it is less sensitive to changes in the bubble size at small radii; as a result, if the prime consideration is to minimise the swelling there is little point in trying to make the bubble radius less than about 5×10^{-7} cm. The swelling is enhanced at higher temperatures; however the Van der Waals term makes this enhancement less pronounced for smaller bubble sizes. Fig.2 shows the number of bubbles per cc as a function of radius for temperatures of 600 and 1200°C: the curve corresponding to T = 1000°C lies between the two curves shown. It is also of interest to note that the pressure of the gas inside the bubbles is often very high. Thus application of Equation 7 shows that $p = 4{\cdot}1 \times 10^{-3}/r$ atmospheres where r is expressed in cm.

For sufficiently large values of swelling, when the gas pressure is low, the bubbles will be so large that they will touch. The gas will then the able to leak out of the solid. Barnes[14] has suggested that in general this will occur when the swelling is 33⅓%, i.e. this should be the largest swelling observed. In fact bigger swellings than this figure have been measured in irradiated fuel elements so that Barnes' analysis may be in error. Nevertheless some maximum possible value for the swelling is to be expected.

It is obvious that considerable swelling of the containment vessel would be an embarrassment in the operation of a reactor. For the purposes of our discussion we shall assume that 10^{-5} cm is the maximum bubble radius corresponding to an acceptable value for the swelling which from Fig.1 is approximately 6%.

3.2.2 An Attempt to Calculate the Swelling and its Dependence on the Temperature of Irradiation

It is evident from Section 3.2.1 that we must calculate the mean bubble size in order to evaluate the swelling. A number of such calculations, based on various simplified models, is discussed below.

3.2.2.1 The Nucleation of Immobile Aggregates During Irradiation and Their Subsequent Growth into Bubbles

This section is based on a treatment due to Greenwood, Foreman and Rimmer[15]. It is assumed that gas atoms are produced randomly in the material at a constant rate during the

irradiation. These atoms will then diffuse until they meet one another by chance encounter and form a pair. It is assumed that very small aggregates (~ 2 He atoms, plus 1 or 2 vacancies to lower the strain energy) are stable and immobile. As the irradiation proceeds the number of such small agregates will build up until the probability that a newly created helium atom will diffuse to an existing aggregate is much greater than that for chance encounter with another helium atom to form a new aggregate. Under these circumstances the aggregates will grow and eventually form bubbles. It may be readily shown that as the aggregates/bubbles growth the probability of new aggregates being created decreases monotonically.

As a result we may imagine that a number of aggegates with an average separation of $2r_1$ are formed initially. The remainder of the helium which is produced will then attach itself to these aggregates and form bubbles, so that each bubble will contain all the helium atoms formed in the spherical region of volume $\frac{4}{3}\pi r_1^3$ around it. As a result if r_1 is known ν_{He}, the number of bubbles per cc may be calculated by means of the simple relation

$$\nu_{He}^{-1} = \frac{4}{3}\pi r_1^3 \qquad \ldots (12)$$

Fig.2 enables the corresponding bubble size to be obtained and this in turn may be used in Fig.1 to read off the value of the swelling.

r_1 remains to be determined. This is given by[15]

$$r_1^6 = \frac{3Dr_o^2a^2}{2GZ} \qquad \ldots (13)$$

where a is the lattice parameter ($3{\cdot}29 \times 10^{-8}$ cm) and r_o the radius of the stable aggregate which is formed initially and assumed here to be 3 Å; G is the production rate of helium atoms ($4{\cdot}35 \times 10^{-12}$ atoms/atomic site per sec) and Z the number of new adjacent sites explored by a gas atom per jump assumed here to be 4. D in Equation 13 is the diffusion coefficient of helium in niobium. Unfortunately its magnitude is unknown, but by analogy with other materials[11] it is reasonable to assume that it is equal to the value of the self-diffusion coefficient. At 600, 1000 and 1200°C these values are $1{\cdot}43 \times 10^{-24}$, $4{\cdot}7 \times 10^{-17}$ and $7{\cdot}6 \times 10^{-15}$ cm^2 sec^{-1} respectively[11]. However allowance must be made for the enhancement of the diffusion due to radiation. This is considered in detail in Appendix 3 and shown to be significant only at 600°C. From the results of Appendix 3 we shall assume therefore that at 600°C the diffusion coefficient is 5×10^{-19} cm^2 sec^{-1}.

Table 2 shows values or r_1, n and the swelling at these three temperatures.

It is evident from Table 2 that the swelling is reasonably small and not very temperature dependent. Further insight into the effect of the different variables on the swelling may be obtained by assuming that the gas in bubbles obeys the perfect gas law. Under these conditions the swelling is proportional to $r_1^{3/2}$, i.e. $\propto\left(\frac{Dr_o^2}{GZ}\right)^{1/4}$.

TABLE 2

Values of half the interbubble separation, the number of gas atoms contained in each bubble and the fractional swelling

Irradiation Temperature ^oC	r_1 cm	n	fractional swelling
600	$5{\cdot}90 \times 10^{-7}$	$1{\cdot}3 \times 10^{2}$	6×10^{-3}
1000	$1{\cdot}26 \times 10^{-6}$	$1{\cdot}3 \times 10^{3}$	7×10^{-3}
1200	$2{\cdot}94 \times 10^{-6}$	$1{\cdot}6 \times 10^{4}$	1×10^{-2}

Thus to increase the swelling by a factor 10 we would have to increase D by a factor 10^4, or r_o by a factor 10^2 or alternatively for the same final gas concentration decrease G by a factor 10^4. It is also clear that any small error in the assumed values of r_o and Z will affect the swelling negligibly. In fact for the bubble sizes predicted here the perfect gas relationship does not hold (see Appendix 2) and it may be shown that the swelling is even less sensitive to changes in the various constantsthan this simplified analysis would indicate.

We are now in a position to demonstrate quantitatively the assertion made in Section 3.2 that the mobility of hydrogen is so large that the formation of aggregates, and hence of bubbles, is a comparatively rare event. For hydrogen in niobium the diffusion coefficient is $1{\cdot}00 \times 10^{-4}$, $5{\cdot}42 \times 10^{-4}$ and $8{\cdot}94 \times 10^{-4}$ cm^2 sec^{-1} at 600, 1000 and 1200^oC respectively[11]; also the hydrogen production rate is $8{\cdot}13 \times 10^{-12}$ atoms/atomic site per second. Using Equation 12 the corresponding values of r_1 were calculated and are shown in Table 3.

TABLE 3

Values of half the bubble separation as a function of temperature for hydrogen in niobium (the simultaneous formation of helium being neglected)

Temperature ^oC	r_1 cm
600	$1{\cdot}28 \times 10^{-4}$
1000	$1{\cdot}70 \times 10^{-4}$
1200	$1{\cdot}85 \times 10^{-4}$

Calculations thus predict that the mean separation of aggregates is about 3 microns. However this calculation assumes that prior to aggregation the hydrogen atoms are migrating in an other wise perfect lattice. In practice the separation of both dislocations and grain boundaries is likely to be approximately of the order of a micron (see Section 3.2.4); as a result hydrogen atoms are likely to reach these sinks rather than form aggregates so that the above analysis is not applicable. Moreover, as already mentioned in Section 3.2, those hydrogen atoms which are able to nucleate and form aggregates will re-dissolve and migrate subsequently to sinks.

3.2.2.2 The Effect of Brownian Motion on the Homogeneous Nucleation of Gas Bubbles

The treatment of Section 3.2.2.1 assumes that stable aggregates and bubbles are immobile. In general this is not true; thus temperature gradients and stress gradients will produce migration (see Sections 3.2.2.3 and 3.2.2.4 respectively). Moreover even if these gradients could be eliminated completely aggregates and bubbles will still migrate owing to Brownian motion. The modification to the simple homogeneous nucleation theory of Section 3.2.2.1 due to Brownian motion which is given here is based on a paper by Greenwood and Speight[16].

Essentially bubbles exhibit Brownian motion because lattice atoms can migrate randomly on their surface (see Appendix 4). The corresponding duffusion coefficient, D_B is given by

$$D_B = \frac{3\nu f a^6}{4\pi r^4} e^{-Q_S/kT} \qquad \ldots (14)$$

where a is the interatomic separation, r the bubble radius, ν the vibrational frequency of atoms, f an entropy factor and Q_S the activation energy for suface diffusion. Values taken for a, ν and f were 2·62 Å, 10^{13} sec^{-1} and unity respectively. Unfortunately no experimental value of Q_S is available at present. However by analogy with other materials it seems reasonable to assume that $Q_S \simeq Q_{gb}$, where Q_{gb} is the activation energy for grain boundary diffusion. Also, by means of a similar argument since no data for Q_{gb} are available, it may be shown that it is reasonable to assume that Q_{gb} is $\frac{2}{3}$ the corresponding Q value for bulk diffusion. Since the latter is 96·0 ± ·9 k.cals/mole[11] the value assumed here for Q_S is 64 k.cals./mole.

The distance moved by a bubble in a time t as a result of Brownian motion is $\sqrt{6D_B t}$. In Fig.3 the distance migrated in 20 years is shown as a function of bubble radius at 600°C, 1000°C and 1200°C. This shows that the distance migrated in 20 years is often extremely small (of atomic dimensions) and decreases rapidly with increasing bubble size.

The results of Table 2 and Fig.3 show that at 600°C Brownian motion of the stable aggregates may be almost entirely neglected. Thus if we assume that the radius of the smallest stable aggregate is 3×10^{-8} cm the time required to migrate a distance $2r_1$ and so coalesce with another aggregate is approximately 0·2 year. However this is slightly longer than the approximate time required for an additional helium atom to be attached to the aggregate which would then become considerably less mobile. As a result at 600°C the simple theory of Section 3.2.2.1 is based on a reasonably realistic model even when Brownian motion is included. Perhaps as a refinement the value of r_o to be used in Equation 12 should be increased slightly, but as we have already seen this should not affect significantly the magnitude of the swelling.

At somewhat higher temperatures the situation is rather more complicated. The smallest stable aggregate can now migrate appreciable distances so that coalescence with other aggregates is likely. Although now less mobile these resulting larger aggregates in their turn will agglomerate further. Eventually when aggregates become sufficiently large they may be considered to be immobile. However the whole process is complicated by the simultaneous production of additional helium atoms. Some of these will attach themselves to the larger aggregates while others, because the agglomeration process decreases the number of aggregates will join together and form more small aggregates.

For this situation Greenwood and Speight[16] have shown that to a first approximation the formation and coalescence of aggregates may be considered to occur during a time t_x given by

$$t_x \sim 0{\cdot}7 \left(\frac{Z}{D}\right)^{5/6} \left(\frac{\gamma\Omega}{kT}\right)^{4/3} \left[\frac{9\nu_D a f Z e^{-Q_s/kT}}{16\pi}\right]^{1/3} G^{-1/2} \qquad \ldots (15)$$

where γ is the surface energy, Ω the atomic volume, ν_D the Debye frequency (assumed to be 10^{13} per sec.) and the other symbols are defined in this section and in Section 3.2.2.1. Subsequently these aggregates grow by the addition of single helium atoms.

At 1000°C $t_x = 7{\cdot}1 \times 10^8$ secs, i.e. just over 20 years so that saturation is not attained. At 1200°C $t_x = 2{\cdot}9 \times 10^7$ sec i.e. ~1 year so that saturation is to be expected.

When saturation has not occurred the fractional swelling is given by

$$\frac{\Delta V}{V} \sim \tfrac{1}{2} \left(\frac{GkTa}{\gamma\Omega}\right)^{6/5} \left[\frac{9\nu_D f Z}{16\pi} e^{-Q_s/kT}\right]^{1/5} t^{7/5} \qquad \ldots (16)$$

where t is the irradiation time. If however $t > t_x$ the fractional swelling is given by

$$\frac{\Delta V}{V} \sim \tfrac{1}{2} \left(\frac{GkTa}{\gamma\Omega}\right)^{6/5} \left[\frac{9\nu_D f Z e^{-Q_s/kT}}{16\pi}\right]^{1/5} \frac{t^{3/2}}{t_x^{1/10}} \qquad \ldots (17)$$

Note that in Equations 16 and 17 the dominant temperature dependent process is Brownian motion (via the activation energy for suface diffusion Q_s) which governs the scale of agglormeration of aggregates. This may be compared with Equation 13 for which Brownian motion was neglected, where the temperature dependent process is the migration of individual helium atoms.

By means of equations 16 and 17 it was found that the fractional swelling at 1000^oC and 1200^oC is about 6×10^{-3} and $2{\cdot}0 \times 10^{-2}$ respectively. Comparison with Table 2 shows that at 1000^oC the swelling is unaffected within the accuracy of the calculations when Brownian motion is taken into account. This is also the conclusion at 600^oC (see above). At 1200^oC there is a doubling in the swelling as a result of Brownian motion, but even so its magnitude is still not too serious. We conclude therefore that in most situations we need not be concerned with the enhancement of the swelling caused by Brownian motion of the bubbles.

3.2.2.3 The Enhancement of Swelling Due to the Presence of Temperature Gradients

Bubbles in a solid which is subject to a temperature gradient will migrate to regions of high temperature. The various mechanisms by which this is possible are discussed in Appendix 4 where it is concluded that in cases which are of interest here the predominant mechanism is the migration of atoms of the solid on the surface. Essentially the temperature gradient results in a net flow of atoms to the lower temperature side of the bubble so that the bubble migrates up the temperature gradient. Equation 18 below shows that for a constant temperature gradient the bubble velocity is inversely proportional to the radius. Consequently an array of identically sized bubbles will migrate at a uniform velocity and no aggregation will take place. In practice a distribution of sizes will be present so that the smaller bubbles will tend to catch up and coalesce with the larger ones. Eventually bubbles will reach such a size that they will be too slow moving to cause further agglomeration and to a first approximation this limiting size will determine the swelling which is to be expected.

The velocity of a bubble of radius r in a solid subject to a temperature gradient $\underline{\text{grad}}\ T$ is[17]

$$\underset{\sim}{v} = \frac{3D_s\Omega^{\frac{1}{3}}Q_s^*}{rkT^2}\ \underline{\text{grad}}\ T \qquad \ldots (18)$$

where Ω is the atomic volume, D_s the surface diffusion coefficient and Q_s^* the heat of transport for surface diffusion. The value of Q_s^* is not known but as discussed by Nicholls[17] it is reasonable to put $Q_s^* = Q_s$, which is taken to be 64 k.cals./mole (Section 3.2.2.2.). D_s is derived from the expression $A \exp\{-Q_s/kT\}$, where the

pre-exponential factor was assumed to be 1·1 cm^2 sec^{-1} by analogy with the value for bulk diffusion. As a result D_s was calculated to be $1{\cdot}3 \times 10^{-16}$, 10^{-11} and $4{\cdot}1 \times 10^{-10} cm^2$ sec^{-1} at 600, 1000 and 1200°C respectively. In order to calculate the temperature gradient to be expected in the containment vessel we note that in the design of Carruthers et al[1] there is a heat flux of approximately 1300 watts cm^{-2} incident upon the walls. If we assume that 15% of this energy is absorbed in the wall and that its thermal conductivity is 0·18 c.g.s. units the maximum temperature gradient is approximately 250°C cm^{-1}.

Fig.4 shows $\underset{\sim}{L}$, the distance migrated in 20 years as a function of radius; values of $\underset{\sim}{L}$ rather than $\underset{\sim}{y}$ are plotted since this quantity is more useful in deciding how much agglomeration occurs. It is evident from Fig.4 that $\underset{\sim}{L}$ varies considerably with temperature and radius.

An exact treatment of the coalescence of bubbles which are nucleating and growing due to irradiation and also migrating up the temperature gradient is rather complicated. In order to simplify the problem let us assume that the helium gas concentration produced after 20 years' irradiation is introduced instantaneously into the niobium in the form of a random array of identical bubbles of radius r. Their concentration will then be given by Fig.2. Let us now anchor all the bubbles except one which is allowed to migrate up the temperature gradient. The average distance the bubble will have to move before meeting another bubble, λ, will be $\frac{1}{\pi\nu r^2}$ where ν is the number of bubbles per cc. Clearly if $L > \lambda$ coalescence will occur within 20 years and the final bubble radius will be greater than r. If on the other hand $L < \lambda$ coalescence will not occur and the size of the bubbles which were formed by the nucleation and growth process (Sections 3.2.2.1 and 3.2.2.2) will be unaffected by the temperature gradient.

Fig.4 shows the value of λ as a function of radius; since the results are not very temperature dependent only values at 600 and 1200°C are shown. It will be noted that for large bubble radii when the perfect gas law is a valid approximation λ is independent of radius. It is evident from Fig.4 that at 600°C bubbles of all sizes are unable to migrate far enough for significant agglomeration to occur. However at 1000 and 1200°C bubbles smaller than about 10^{-5} and 10^{-4} cm radius respectively will be able to agglomerate. Since this value is greater than the size of bubbles formed by the nucleation and growth process (Sections 3.2.2.1 and 3.2.2.2) the temperature gradient will result in bubble aggregation so that the final bubble size is of the order of 10^{-5} and 10^{-4} cm at 1000 and 1200°C respectively. From Fig.1 this corresponds to an approximate fractional swelling of 6 and 70%.

However, as has already been emphasised, the above is a highly simplified treatment of what may occur in the containment vessel. In fact the mean free path for coalesence will be larger than that calculated here for three reasons. Firstly the helium concentration will only attain the value which is used in the calculations at the end of the 20 year irradiation. Secondly all the bubbles are moving in the same direction up the temperature gradient. As a result the mean free path for coalescence depends on the relative velocity of bubbles which in turn depends on the bubble size distribution. Thirdly we assumed that in the containment vessel the temperature gradient is uniform over the wall thickness i.e. that all the energy absorption occurs on the inner surface of the wall. Since this is clearly not the case the temperature gradient and hence the swelling will not be as large as is indicated above in the material close to the inner wall radius.

The results of this discussion show that at 600°C there should be no swelling problems arising from temperature gradients which are likely to be encountered. We conclude that at 1000 and 1200°C enhancement of the swelling due to temperature gradients occurs, its value being about 3 and 30% respectively; clearly it is in this temperature region that the value of the swelling becomes unacceptably large.

3.2.2.4 The Enhancement of Swelling Due to the Presence of Stress Gradients

In a manner analogous to that relating to temperature gradients, stress gradients can also produce bubble migration with a consequent possibility of agglomeration and enhanced swelling. In order to investigate the importance of this effect the present author had first to derive an analytical expression for the velocity of a bubble in a stress field since the expressions published in the literature appeared to be inappropriate for the present application. Since a detailed derivation of this expression and its general implications have been published elsewhere[18] only the principles of evaluating the velocity of a bubble in a stress gradient and its application to the present problem will be given here.

First we must calculate the driving force on a bubble in a stress gradient. We make the basic assumption that bubbles are always in equilibrium (Appendix 1); when a hydrostatic stress is present Equation 6 is modified to

$$p - \sigma_c = \frac{2\gamma}{r} \qquad \ldots (19a)$$

and

$$p + \sigma_t = \frac{2\gamma}{r} \qquad \ldots (19b)$$

for compressive stresses σ_c and tensile stresses σ_t respectively. We also assume that the gas obeys the simplified Van der Waals expression of Equation 10.

The force on a bubble in a stress gradient may be calculated from the work done by the bubble as it moves a small distance in the solid. There are two contributing factors to consider: (a) the work done on the solid by the bubble due to its corresponding change in volume, and (b) the change in strain energy stored in the solid.

It may be shown that only for very small bubbles, with radii smaller than about 10^{-7}cm does the term corresponding to mechanism (b) attain any importance. Since our main concern here is with bubble sizes which are larger than 10^{-7} cm in radius we may therefore neglect this term. The physical meaning of this is that much more energy is stored per unit volume in the gas than in the solid owing to its greater compressibility. The driving force due to mechanism (a) is

$$\underset{\sim}{F} = - \frac{4\pi r^4 \sigma_c}{4\gamma + 3\sigma_c r + \frac{3brp^2}{kT}} \underline{\text{grad}}\ \sigma_c \qquad \ldots (20a)$$

and

$$\underset{\sim}{F} = - \frac{4\pi r^4 \sigma_t}{4\gamma - 3\sigma_t r + \frac{3brp^2}{kT}} \underline{\text{grad}}\ \sigma_t \qquad \ldots (20b)$$

for compressive and tensile stresses respectively. It will be noted from the signs of the expressions that bubbles will be driven towards regions of lower stress irrespective of whether the solid is under compression or tension.

Finally the distance a bubble migrates in time t is given by[17]

$$\underset{\sim}{L} = \frac{3D_s \Omega^{4/3} t}{2\pi r^4 kT} \underset{\sim}{F} . \qquad \ldots (21)$$

In order to estimate the importance of this effect we need first of all to calculate some typical values of the stresses and stress gradients which are likely to be encountered in the containment vessel.

To a first approximation we can consider the vessel as a very long hollow cylinder subject to a temperature distribution with cylindrical symmetry. Timoshenko and Goodier[19] have given the corresponding stress components when the ends of the cylinder are restrained but (as in a toroid allowed to expand freely) the resultant forces are zero. The effective hydrostatic stress which is of concern here is simply one third the sum of these three components. Hence

$$\sigma = \frac{\alpha E}{3(1-\nu)} \left[\frac{4}{b^2 - a^2} \int_a^b Tr dr - 2T \right] \qquad \ldots (22)$$

where α is the coefficient of expansion, E the elastic modulus, ν Poisson's ratio,

a and b the inner and outer radii of the cylinder, and T the temperature. Since the thickness t of the cylinder is very much smaller than a or b, Equation 22 may be approximated to a simpler expression

$$\sigma(x) = \frac{2\alpha E}{3(1-\nu)}\left[\frac{1}{t}\int_0^t T dx - T\right] \qquad \ldots (23)$$

In order to calculate T as a function of radial distance in the wall we shall assume an infinite plane slab geometry. We shall also assume that the heat absorbed in the wall per unit time may be divided into two components: (a) an amount Q per unit area deposited in an infinitesimal thickness on the inner surface (e.g. due to Bremsstrahlung and cyclotron radiation from the plasma) and (b) a uniform heating H per unit volume throughout the material. As a result the temperature in the wall as a function of distance x from the inner surface is

$$T = T_i - \frac{Qx}{k} - \frac{Hx^2}{2k} \qquad \ldots (24)$$

where T_i is the temperature of the inner surface and k the thermal conductivity. Let us make the further simplification that the heat deposited on the surface and in the volume of the material are equal, i.e. Q = Ht. Hence from Equations 23 and 24

$$\sigma(x) = \frac{2\alpha EQ}{3(1-\nu)k}\left[x + \frac{x^2}{2t} - \frac{2t}{3}\right] \qquad \ldots (25)$$

and the stress gradient is given by

$$\frac{d\sigma}{dx} = \frac{2\alpha EQ}{3(1-\nu)k}\left[1 + \frac{x}{t}\right] \qquad \ldots (26)$$

The largest values of σ and $\frac{d\sigma}{dx}$ occur at the inner and outer surfaces, where the stresses are compressive and tensile in nature respectively. The maximum numerical values occur on the outer surface. If 1300 W cm^{-2} of energy are incident on the wall, 15% of which is absorbed and with $\alpha = 7{\cdot}6 \times 10^{-6}$ deg.$^{-1}$, $E = 1{\cdot}05 \times 10^{12}$ dynes cm^{-2}, $\nu = 0{\cdot}40$, $k = 0{\cdot}60$ W cm^{-1} deg.$^{-1}$ and $t = 2$ cm we find that for $x = t$ $\sigma = 2{\cdot}56 \times 10^9$ dynes cm^{-2} and $\frac{d\sigma}{dx} = 3{\cdot}07 \times 10^9$ dynes cm^{-3}.

Fig.5 shows the value of L at 1000°C calculated from Equation 20 for a time of 20 years. Results for three values of compressive stresses are shown to indicate the effect of variations in stress. As L is directly proportional to the stress gradient only results with $\frac{d\sigma}{dx} = 3 \times 10^9$ dynes cm^{-3} are shown. A curve analogous to that in Fig.4 showing the mean free path for coalescence as a function of bubble radius but for T = 1000°C is also shown. It is evident from the non-intersection of the two types of curves that

under no circumstances will there be a significant amount of coalescence due to the migration of bubbles in the stress field.

Curves of L as a function of bubble radius under conditions of tensile stress are not shown here since they are complicated by catastrophic bubble growth effects (see Section 3.2.6). It is sufficient for our present pruposes to observe that for the same numerical values of σ and $\frac{d\sigma}{dx}$ values of L are comparable under compression and tension. A justification of this conclusion together with a more detailed treatment of the motion of bubbles in tensile stresses is given by the author in reference 18.

The results in Fig.5 were calculated at $1000^{o}C$. At $600^{o}C$ it is evident that coalescence is even less likely. At $1200^{o}C$ the values of L must be multiplied throughout by 35 so that there is a chance of coalescence near the surfaces of the wall for bubble sizes smaller than about 10^{-6} cm. However this should not affect the magnitude of the swelling appreciably. Moreover, as explained in the penultimate paragraph of Section 3.2.2.3, the distance a bubble migrates before coalescence occurs will be larger than the value of λ shown in Fig.5.

It is evident therefore that the migration of bubbles due to stress gradients will have a negligible effect on the magnitude of the swelling.

3.2.3 The Possibility of Reducing the Swelling by Means of a Hydrostatic Compressive Stress

Let us reconsider the situation of Section 3.2.1, where the swelling was calculated as a function of bubble size and the results shown in Fig.1. Suppose now that the solid-gas bubble ensemble is compressed hydrostatically. In order to maintain the bubbles in equilibrium their radii must decrease and so there will be an attendant decrease in the magnitude of the swelling. If r_i is the bubble radius before the stress is applied and p_i the gas pressure we may rewrite equation 7 as

$$p_i = \frac{2\gamma}{r_i} \qquad \ldots (27)$$

If p and r are the pressure and radius when a compressive stress σ is applied then the condition for equilibrium is[20]

$$p = \frac{2\gamma}{r} + \sigma \ . \qquad \ldots (28)$$

Assuming that the helium obeys the perfect gas law

$$p_i r_i^3 = p r^3 = \text{constant} \qquad \ldots (29)$$

it follows immediately that

$$\sigma = \frac{2\gamma}{r}\left[\left(\frac{r_i}{r}\right)^2 - 1\right]. \qquad \ldots (30)$$

Now if Δ_i and Δ denote the swelling before and after the stress is applied

$$\frac{\Delta_i}{\Delta} = \left(\frac{r_i}{r}\right)^3 \qquad \ldots (31)$$

so that

$$\sigma = \frac{2\gamma}{r_i}\left[\frac{\Delta_i}{\Delta} - \left(\frac{\Delta_i}{\Delta}\right)^{\frac{1}{3}}\right] \qquad \ldots (32)$$

Fig.6 shows Δ as a function of σ for three values of r_i. Values of Δ_i, corresponding to $\sigma = 0$, are taken from Fig.1.

It is evident that comparatively modest stresses can result in a significant reduction in the swelling when Δ_i is high. However the fact that the various curves converge at higher stresses means that if it is desired to reduce the swelling to a certain figure the value of σ that is required is often not a very sensitive function of Δ_i. For example, to reduce the swelling to 6% requires stresses of about 5,000 and 6,000 for Δ_i values of 60 and 600% respectively.

It should be noted that for the sake of simplicity the perfect gas law was assumed throughout these calculations. Let us suppose that the deviation of the equation of state from the perfect gas law is only significant for pressures greater than about 4×10^9 dynes cm^{-2}; this figure was arrived at from the point where significant deviations from straight lines of the curves in Fig.1 occur, when the corresponding bubble radius is 10^{-6} cm. At such pressures it may be shown that for the bubble sizes employed in Fig.6 it is permissible to put $\rho \sim \sigma$, which implies that significant deviations from the perfect gas law occur for swellings less than about 1%. As a result the swelling for specific values of σ is significantly too low in Fig.6 when $\Delta \lesssim 10^{-2}$.

The results shown in Fig.6 all relate to $1000^{\circ}C$. Curves corresponding to 600 and $1200^{\circ}C$ are nearly parallel to the $1000^{\circ}C$ results, the swelling values being modified by factors similar to those between the different curves of Fig.1. As a result the conclusions derived above are not very dependent on the temperature.

We must now discuss the effect that a hydrostatic stress applied to the containment vessel would have on the swelling; i.e. we must consider in addition the nucleation, growth and migration of bubbles under stress.

The nucleation and growth of immobile bubbles, in accordance with the theory of Section 3.2.2.1 should essentially be unaffected. The diffusion constant D in Equation 12 which

describes the migration of individual helium atoms may be slightly decreased - say by not more than 10% - as a result of the applied stress. However since we have seen that the swelling is dependent upon $D^{\frac{1}{4}}$ this should not affect the conclusions of Section 3.2.2.1 significantly (apart from the fact that bubbles are now smaller, as discussed above).

From Section 3.2.2.3 we have seen that the temperature gradient is the most important mechanism by which bubbles migrate and hence coalesce to give a higher swelling value than that predicted by the simple theory of Section 3.2.2.1. When a hydrostatic stress is applied three additional factors must be considered: (a) D_s, the surface diffusion coefficient may be altered. No experimental information about this effect is known, but one might expect D_s to decrease with stress. (b) Since for a given number of helium atoms contained in a bubble its radius will be smaller the distance migrated in 20 years will be greater under stress (see Equation 18). (c) Since the volume fraction of the solid which contains helium is less the mean free path for coalescence will be greater. A detailed analysis of these three factors is somewhat complex; however to a first approximation we can perhaps say that (a) is unimportant while (b) and (c) will tend to cancel each other out. As a result the final mean bubble size will hardly be affected by the stress. However, if we assume that the bubble radius remains unchanged, the fractional decrease in the swelling, φ, will, from Equation 28, be

$$\varphi = \left(1 + \frac{\sigma r}{2\gamma}\right)^{-1} \qquad \ldots (33)$$

since the gas pressure will be enhanced. (Physically this means that there are more helium atoms per bubble and fewer bubbles per cc). For example the swelling will be halved if the pressure is $\frac{6{\cdot}1 \times 10^{-2}}{r}$ p.s.i. where r is in cm. We note that for large values of $\frac{\Delta_i}{\Delta}$ ($= \varphi^{-1}$) Equations 32 and 33 tend to become equal.

We conclude therefore that the application of hydrostatic stresses is capable of significantly reducing the swelling; the desirability and feasibility of applying such stresses is of course another question. However the point to be brought out here is that if intolerably large swellings are anticipated then the application of a hydrostatic compressive stress should be considered as a possible way of reducing it to reasonable values.

3.2.4 The Effect of Dislocations and Grain Boundaries on the Swelling Calculations

Hitherto we have assumed in the calculations that prior to irradiation the niobium lattice is perfect. In fact the various imperfections which will occur in it are bound to affect the number and size of bubbles and hence the swelling; we consider here the importance of this effect.

Impurity atoms in the lattice e.g. due to substitutional solid solution are most unlikely to affect the results significantly for two reasons: (a) the strain fields around impurity atoms are often small (see also below); as a result they should not affect significantly the migration of helium atoms by trapping[21]. (b) Since bubbles are significantly larger than atomic dimensions single impurity atoms are unable to affect the migration of bubbles, as discussed in Sections 3.2.2.2-3.2.2.4.

The possibility of bubbles being trapped on dislocations or grain boundaries is potentially of much greater importance since they can migrate more rapidly along dislocation lines or in grain boundaries than untrapped bubbles in the perfect crystal; as a result coalescence and hence swelling may be significantly enhanced compared with a perfect crystal.

First let us consider the preferential nucleation of bubbles close to dislocations due to the strain field attraction between the gas atoms and the dislocation. (Note that no comparable mechanism occurs for grain boundaries). It has often been asserted in the literature that the vicinity of dislocations is a highly favoured region for the nucleation of bubbles. These assertions are based on Greenwood, Foreman and Rimmer's paper[15] where the nucleation of xenon bubbles following the fission of uranium is considered. They showed that owing to strain field interactions xenon atoms are attracted into the dislocation on the tensile side; as a result when the gas atom distribution attains equilibrium the concentration 10^{-7} cm from the dislocation core is enhanced by a factor 10^5 compared with that in a region of stress free material. In addition the time required for this equilibrium concentration (which varies with distance from the core) to be established is comparable to the time required for nucleation of bubbles in the stress free regions of the crystal. As a result Greenwood, Foreman and Rimmer concluded that a large fraction of the bubbles would be nucleated very close to dislocations. Moreover as they grew and also migrated we would expect to find that these bubbles are eventually trapped on the dislocation lines.

However somewhat different conclusions are arrived at here. Firstly we note that the enhancement factor in the gas concentration around a dislocation is related to the strain energy of gas atoms by the respective radii of the gas and matrix atoms. Since the atomic radius of helium is about half that of xenon[5] the corresponding strain energy should be less and the enhancement factor orders of magnitude lower (or possibly there is no enhancement at all, see below). For example, Rimmer and Cottrell[22] have estimated the energies of the inert gases on interstitial and substitutional sites in copper. They found that for

a helium interstitial the strain energy is 1·7 eV; for a xenon interstitial the corresponding energy is 21 eV while if it is in a substitutional site the energy is 5·8 eV. Moreover Rimmer and Cottrell suggested that while in isolation helium will be located preferentially on interstitial sites, it will become substitutional with a strain energy of zero if vacancies are also present; experimental evidence would appear to support this conclusion[81]. Unfortunately no comparable calculations are available for niobium; however it is evident that strain fields must be much smaller for lower atomic number gas atoms and in the case of helium may be zero. Mention should be made that an accurate calculation would require also a term for the change in energy of electrons near the defects; this is normally smaller than the strain energy.

Considering now the time required for the equilibrium distribution to be set up, this is given by[15] $\tau_d \sim d^2/D$ whereas the time required for two helium atoms to meet and form a nucleus is given by $\tau_n \sim r_o a^2/2Gr_1^3Z$, where d is the dislocation spacing and the remaining symbols are defined in Section 3.2.2.1. For a dislocation density of 10^8 lines cm^{-2} $\tau_d \sim 2 \times 10^{10}$, 2×10^8 and 2×10^6 secs at 600, 1000 and 1200°C respectively; in comparison τ_n, which is not a very sensitive function of temperature is about 10^6 secs. As a result at 600 and 1000°C $\tau_d \gg \tau_n$, while at 1200°C τ_d is slightly larger than τ_n. Hence at 600 and 1000°C little nucleation will occur near dislocations. At 1200°C some preferential nucleation may occur. However as the bubbles which are formed in the perfect crystal grow they have a greater probability of absorbing the newly created gas atoms. Note also that the value of d which is assumed in the above calculations is probably on the low side for an annealed crystal. This is because although 10^8 lines cm^{-2} is a reasonable mean value for the dislocation density in an annealed material these are often distributed inhomogeneously[23]. As a result it is reasonable to assume that the effective line density is one or two orders of magnitude less and this will enhance τ_d by the same factor. This would result in appreciable nucleation near dislocations being unlikely even at 1200°C.

We conclude therefore that in contrast to the problem considered by Greenwood, Foreman and Rimmer[15] there is little preferential nucleation of bubbles close to dislocation lines. The differences between the two cases are that xenon is attracted more strongly by the stress field of a dislocation than is helium and the relative values of τ_d and τ_n are different, mainly because the diffusion coefficient assumed for niobium is smaller than that of uranium; essentially this is because the envisaged temperature of the niobium in a containment vessel is a smaller fraction of the melting point than that of the uranium fuel in a fission reactor.

We now consider the possibility that bubbles may migrate to and be trapped by dislocations. Although under certain circumstances a repulsive force occurs between bubbles and dislocations[18] it can be ignored to a first approximation since this is smaller than the driving force due to temperature gradients.

The mean free path λ_d for a migrating bubble to reach a dislocation is given by $\lambda_d \sim (2r\nu)^{-1}$ where ν is the number of dislocation lines per cm^2; clearly this decreases with bubble size. On the other hand the mean free path for bubbles to aggregate λ_{agg} which is shown in Fig.4 (as λ) tends to a constant value for large radii. Consequently, assuming that bubbles are mobile, there is a critical radius below and above which aggregation and trapping on dislocations are favoured respectively. By taking $\lambda_d = \lambda_{agg}$ we find that for $\nu = 10^8$ and 10^6 lines cm^{-2} the critical radii are $\sim 2 \times 10^{-5}$ and 2×10^{-3} cm respectively. (Since the λ_{agg} values shown in Fig.4 are too low (Section 3.2.2.3) these values of the critical radius have been overestimated.) Now we know that bubble radii greater than about 10^{-5} cm cannot be tolerated (Section 3.2.1); as a result bubble migration which is of interest here will result in hardly any of them arriving at dislocations.

We now consider the possibility that bubbles are trapped on grain boundaries. Assuming that a typical value for the grain diameter is 20 μm, bubbles must migrate on average $\sim 10^{-3}$ cm for trapping to be likely. If bubbles migrate entirely as a result of temperature gradients (which we have seen to be the dominant mechanism) it is evident from Fig.4 that at 600°C bubbles of all sizes migrate much less than 10^{-3} cm so that trapping may be neglected. At 1000°C however bubbles migrate further than 10^{-3} cm if $r < 2 \times 10^{-6}$ cm. However since λ (Fig.4) is always smaller than 10^{-3} cm bubbles will normally coalesce before reaching grain boundaries. The larger bubbles so formed will then be less mobile and as a result will not generally reach grain boundaries. At 1200°C bubbles up to about 8×10^{-5} cm in radius should migrate to grain boundaries so that these may affect the swelling.

However if bubbles are larger than a certain size the driving force due to the temperature gradient will exceed the restraining force of the grain boundary; as a result bubbles will be torn off boundaries and continue to migrate through the lattice. The requirement for this is[17]

$$\frac{2\pi r^3}{\Omega} \frac{Q_S^*}{T} \text{ grad } T > \pi r \gamma_{gb} \qquad \ldots (34)$$

where the left and right hand sides of this inequality correspond respectively to these forces. γ_{gb} denotes the grain boundary surface energy, assumed here to be 300 ergs cm^{-2}[17]. As a result, if $r \gtrsim 5 \times 10^{-5}$ cm bubbles will be torn off grain boundaries. Since this is

about the bubble size which was predicted at 1200°C assuming a perfect lattice it appears therefore that the size is not greatly affected by the presence of grain boundaries although the method by which the bubbles grow may be different (e.g small bubbles may collect on grain boundaries, coalesce until they are $\sim 5 \times 10^{-5}$ cm in radius and then migrate through the lattice).

Finally we note that although most bubbles do not reach dislocations, it may be shown that those which do will be torn off when the radius $\gtrsim 10^{-5}$ cm using arguments similar to those presented above for grain boundaries.

In conclusion therefore the presence of impurities, dislocations and grain boundaries have little influence on the swelling calculated for a perfect lattice. Perhaps at 1200°C there may be some enhancement of the swelling due to the migration of bubbles on grain boundaries.

3.2.5 The Re-solution of Bubbles by Neutron Irradiation

In fissile materials it is believed that bubbles formed by the aggregation of gaseous fission products may be dissolved subsequently by the radiation[24]. Bubbles in non-fissile materials will also dissolve under irradiation, although at a slower rate. Clearly it is important for us to consider whether in the present application a significant fraction of the helium will be dissolved in the lattice since if this is so many of the bubble calculations described above will need to be modified.

Turnbull[25] has suggested that there are four mechanisms by which bubbles in UO_2 may be redissolved by radiation. Expressed in terms appropriate to non-fissile materials these are:

1. The transfer of energy by the collision of a fast neutron with a gas atom contained in a bubble; the atom then dissipates its energy by travelling some distance through the solid.
2. Same as 1 except that the collisions are caused by energetic primary knock ons which pass through the bubble.
3. Same as 1 except that collisions are caused by atoms in the collision cascade (produced as the primary knock on dissipates its energy) as they pass through the bubble.
4. The transfer of energy to many atoms in a collision cascade results essentially in a certain volume being heated to a high temperature for a short time. If this region, known as a thermal spike, is close to a bubble surface some of the solid will be evaporated and recondense on the opposite side of the bubble. Re-solution will occur since some gas atoms in the bubble will be trapped inside the condensed material.

For bubbles in UO_2 Turnbull[25] has calculated the value of b, which is defined as the atomic fraction of gas atoms in bubbles which is dissolved per second, for each of the four above mechanisms.

The value of b corresponding to mechanism 1 is approximately equal to $\varphi\sigma$, where φ is the neutron flux and σ the neutron-gas atom cross section. Taking these as 4×10^{14} neutrons cm^{-2} sec^{-1} and 10^{-24} cm^2 respectively b is approximately 4×10^{-10} atomic fraction per second.

Calculations of b for mechanisms 2-4 are rather more complex. However by means of suitable scaling parameters Turnbull's results may be applied directly to the present problem.

The mean energy of a primary knock on in niobium is 181 keV (Table 5); this is to be compared with an energy of about 80 MeV for a fission fragment, i.e. the energy ratio is $\sim 2 \times 10^{-3}$ and this is also the approximate ratio of their ranges (of the order 10^2 and 10^5 Å respectively). By means of qualitative arguments it may be shown reasonable to assume that the chances of mechanisms 2, 3 and 4 occurring are proportional to the range of the primary. Hence Turnbull's figure of b for mechanisms 2, 3 and 4 must be multiplied by 2×10^{-3}.

There are however two other factors to be taken into account. Since primaries in non fissile material possess much less energy than fission fragments their efficiency in producing re-solution will be less (essentially because the lattice is disturbed less). In addition for the neutron flux considered here the number of primary knock ons per cc per second in niobium ($\sim 10^{14}$) is about three times the number of fission fragments per cc per second assumed by Turnbull in his calculations. Since these two factors tend to cancel each other we will ignore them and assume that the appropriate factor is 2×10^{-3}. However we note that this factor will be too high since the re-solution efficiency factor must be much less than ⅓.

Finally, by scaling Turnbull's results for mechanisms 2-4 we find that the values of b relating to mechanisms 1-4 are 4×10^{-10}, 2×10^{-10}, 10^{-9} and 5×10^{-9}, so that the overall values of b is 7×10^{-9} atomic fraction per second. This means that an isolated bubble in an otherwise perfect infinite solid will lose half its gas atoms in about 10^8 sec = 3 years.

We now enquire how important this re-solution is on the results presented above, where this effect was ignored. There are two reasons which lead us to conclude that re-solution may be neglected. Firstly we have seen that b is overestimated, i.e. the

re-solution rate is smaller than that calculated. Clearly if the time required for half the atoms in a bubble to dissolve greatly exceeds 20 years the effect may be neglected. Secondly even if we accept the calculated value of b bubbles will appear to dissolve imperceptibly since the gas atoms which are knocked into the lattice will rapidly diffuse back to bubbles. Thus if $2r_1$ is the separation between bubbles the time required for a helium atom to diffuse back to a bubble will not exceed approximately r_1^2/D, where D is the diffusion coefficient. Using the values of r_1 and D given in Section 3.2.2.1 we find that at 600, 1000 and 1200°C these times are about 7×10^5, 3×10^4 and 10^3 sec respectively. Since they are considerably shorter than 10^8 sec, the time for half the gas to be dissolved, it is evident that at any instant only a minute fraction of all the gas atoms are not contained in bubbles.

We conclude therefore that the re-solution of gas atoms by radiation may be neglected for all practical purposes.

3.2.6. The Catastrophic Growth of Bubbles and Subsequent Fracture of the Solid under a Tensile Stress

In Section 3.2.3 it was pointed out that if a compressive stress was applied to a solid containing bubbles these will decrease in radius in order to remain in equilibrium. Conversely if a tensile stress is applied the bubbles will grow; an analysis of this situation is identical to that leading up to Equations 27-30 except that the sign of σ is changed. As a result Equation 30 may be re-written as

$$\sigma = \frac{2\gamma}{r}\left[1 - \left(\frac{r_i}{r}\right)\right]^2 \qquad \ldots (35)$$

where σ is the tensile stress and r_i the bubble radius when $\sigma = 0$. Differentiating this expression we find that

$$\frac{d\sigma}{dr} = \frac{2\gamma}{r^2}\left[3\left(\frac{r_i}{r}\right)^2 - 1\right]. \qquad \ldots (36)$$

Clearly when σ is small and $r \sim r_i$ $\frac{d\sigma}{dr}$ is positive, giving the result stated above that the equilibrium radius of the bubble increases with the tensile stress. However if the stress is steadily raised until $r = \sqrt{3}\, r_i$ $\frac{d\sigma}{dr}$ becomes zero, i.e. the bubble will expand indefinitely and so will never attain equilibrium. The critical stress value, σ_{crit} at which this occurs is obtained from Equation 35 with $r = \sqrt{3}\, r_i$:

$$\sigma_{crit} = \frac{4\gamma}{3\sqrt{3}r_i} \qquad \ldots (37)$$

Fig.7 shows σ_{crit} as a function of radius. Clearly if $\sigma \geq \sigma_{crit}$ bubbles can join up as they grow and a fissure be formed across the solid, so that fracture will take place. However the relation $\sigma \geq \sigma_{crit}$ is a necessary but not sufficient condition for fracture.

In addition the bubble growth, which is controlled by the vacancy flow, must occur sufficiently quickly for fracture to occur in times of practical interest. Because vacancies are much more mobile along grain boundaries than in the bulk of the material, it may be assumed that the small fraction of bubbles lying on grain boundaries will grow preferentially, and so form the plane along which fracture will occur.

Hull and Rimmer[26] have considered what is essentially the same problem, namely the time required for fracture due to voids on grain boundaries expanding as a result of a tensile stress. The only modification required when their results are applied to bubbles is to ignore all situations for which the applied stress is less than σ_{crit}. The time for fracture is given by the relation

$$t = \frac{a_v^3 kT}{16\pi\sigma\Omega D_{gb}\delta_Z} \qquad \ldots (38)$$

where a_v is the spacing of bubbles on the grain boundary, Ω the atomic volume, D_{gb} the grain boundary diffusion coefficient and δ_Z the width of the grain boundary.

Equation 37 contains two simplifications: (a) It is assumed that σ remains constant whereas in fact as the bubbles grow the effective stress will increase; when bubbles nearly touch there will be plastic deformation in the material between them. (b) Bubbles are assumed to be uniformly spaced. In fact the time for fracture will be dominated by those bubbles which are more widely spaced. Since it is hard to allow for these two effects they will be neglected. We note however that they will tend to cancel each other out.

If we assume that a fraction f of the bubbles lie on grain boundaries the mean spacing of these is given by the expression

$$a_v^2 \simeq \frac{3}{f\nu d} \qquad \ldots (39)$$

where d is the grain diameter and ν the number of bubbles per cc (see Fig.2). We will assume that 1% of all the bubbles occur on grain boundaries and that the grain diameter is 50 μm[26].

No experimental values of D_{gb} are available. Instead we shall assume that values of D_{gb} are the same as those for the surface diffusion coefficient which were discussed above i.e. the pre-exponential factor was taken to be 1·1 $cm^2\ sec^{-1}$ (Section 3.2.2.3) and the activation energy 64 kilo calories per mole (Section 3.2.2.2). As a result at 600, 1000 and 1200°C $D_{gb} = 1{\cdot}3 \times 10^{-16}$, 10^{-11} and $4{\cdot}1 \times 10^{-10}$ $cm^2\ sec^{-1}$ respectively. We shall also assume that δ_Z is 5×10^{-8} cm[11]. Using this data Equation 37 has been used to calculate the stress required for fracture to occur in 20 years and this is shown at temperatures of 600, 1000 and 1200°C in Fig.7. In addition a horizontal line has been

drawn in Fig.7 at 10,000 psi to indicate an approximate value of the yield strength of niobium at these temperatures.

It is evident that the region of the figure which is of concern to us lies above the σ_{crit} line (since below this line bubbles will not expand indefinitely), below the yield strength line (since a vessel containing higher stresses cannot be fabricated) and also for stresses greater than that required for fracture to occur after 20 years, i.e. within the triangle bounded by these three lines. As a result, at 600°C fracture cannot occur, irrespective of the applied stress and bubble size. However at 1000°C fracture is possible for bubble sizes between 2×10^{-6} and $1{\cdot}8 \times 10^{-4}$ cm. The lowest fracture stress is 500 psi, corresponding to a bubble radius of 6×10^{-5} cm. At 1200°C this minimum stress is 160 psi, corresponding to a radius of $1{\cdot}4 \times 10^{-4}$ cm; also the upper bubble radius for the fracture stress to equal the yield stress is 6×10^{-4} cm.

Bearing in mind that the bubble radius at 1000 and 1200°C is about 4×10^{-6} and 4×10^{-5} cm respectively (see Section 3.2.2.3) these results suggest that fracture can occur within 20 years if the stress is greater than about 6,000 and 600 psi respectively. However it should be emphasised that the calculation of the stress for failure to occur in 20 years is somewhat approximate and while any errors in the calculation may increase these critical stresses they will not lower them. In addition creep considerations (Section 4.4) will probably demand lower stresses than the above limiting values. As a result fracture due to catastrophic bubble growth will probably not be a limiting factor; nevertheless this effect should be borne in mind in any specific design studies. Of course if the containment vessel could be fabricated such that all the stresses associated with it are compressive no possibility of fracture occurs.

4. THE EFFECT OF DISPLACEMENT DAMAGE ON THE PROPERTIES OF NIOBIUM

Many studies of the displacement or radiation damage of materials by neutrons have been performed in the past. However for the purpose of application to the present assessment they suffer from three drawbacks: (a) The neutron sources used in these studies have been almost exclusively fission reactors, for which close to fuel elements the neutron energy is peaked at around 1 MeV. Even allowing for neutrons being backscattered with degraded energy their mean energy in the wall of a thermonuclear reactor is likely to be considerably higher than this; furthermore an appreciable fraction of the neutrons passing through the wall will possess an energy of 14·1 MeV. Although the radiation damage produced by, say a 14·1 MeV neutron compared with one of 1 MeV may be calculated (see Section 4.1) the corresponding changes in the physical properties cannot be simply scaled accordingly

owing to the difference in the spatial distribution of the damage and its different annealing characteristics. (b) The neutron doses which are of concern to us are extremely high; as a result comparatively few radiation damage studies at such doses have been reported. (c) The gas production rate is much greater at 14·1 MeV than at 1 MeV. This may well affect some of the displacement damage effects (see Section 6.2).

It is inevitable therefore that the conclusions drawn in this section are often somewhat speculative.

4.1 A Comparison Between the Radiation Damage Produced by a 14.1 MeV Neutron and one with an Engery of 1 MeV

The present treatment follows closely that given by Odette[27], who considered copper and molybdenum.

The maximum energy T_{max} given to an atom of mass M (expressed in atomic mass units) by a neutron of energy E_n is given by

$$T_{max} = \frac{4M}{(M+1)^2} E_n \qquad \ldots (40)$$

As a result for $E_n = 1$ and 14·1 MeV T_{max} in niobium is 42·1 and 594 keV respectively.

In order to calculate the probability that an atom will receive an energy T we require to consider the cross sections for the various possible interactions at the two energies. Table 4 shows the total cross sections which are used in the calculations.

TABLE 4

Some total cross sections of niobium for neutrons with energies of 1 and 14·1 MeV. Values are in mbarn.

Process	1 MeV	14·1 MeV
All interactions	6700[4]	3940[28]
Elastic scattering	6220[4]	1770[28]
Non-elastic scattering	660[4]	2170[28]

The energy T imparted to an atom is related to the angle through which the neutron is scattered, θ, by the relation

$$T = \tfrac{1}{2} T_{max}(1 - \cos\theta) \qquad \ldots (41)$$

In Equation (41) we have made the good approximation that the scattering angle is identical in laboratory and centre of mass co-ordinates. We now require to calculate the elastic differential scattering cross section $K_e(E_n,T)$; normally differential cross

sections as a function of the cosine of the scattering angle, i.e. $k_e(E_n, \cos\theta)$ are quoted[28,29]. The two are related by the equation

$$K_e(E_n, T) = \frac{4\pi}{T_{max}} k_e(E_n, \cos\theta) \qquad \ldots (42)$$

(the relationship between T and $\cos\theta$ being given by Equation (41)).

Since in comparison a rigorous description of the various non-elastic scattering processes is more difficult we shall instead resort to an approximate treatment.

The inelastic cross section is obtained by summing over the various excited states of the nuclei as, for example, was done by Hyder and Kenward[30] for a fission reactor neutron spectrum. For higher energies ($\gtrsim$ 5 MeV) the excited levels become so closely spaced that it is more convenient to use a statistical model based on nuclear evaporation theory[31]. In addition experimental data indicate that the inelastic scattering is very nearly isotropic. For simplicity we shall in fact treat the inelastic scattering as though it were both elastic and isotropic. This should not be too bad an approximation at low energies ($\sim$ 1 MeV) since the inelastic scattering is only a small fraction of the total scattering; also although it will overestimate the average energy given by 14 MeV neutrons to primaries this will not be as serious as the nuclear evaporation theory would indicate since theory is known to underestimate the number of scattering events which result in the nucleus being excited to comparatively low energy levels. In addition we shall ignore the recoil energy given to an excited nucleus as it decays to the ground state by γ emission since this will normally be much smaller than the energy imparted to it by the inelastic scattering event.

To a good approximation the inelastic cross section at 1 MeV may be equated with the non-elastic cross section since the next most important interaction, the (n,γ) reaction, has a cross section of only 35 mbarn. At 14 MeV however there is a sizeable contribution to the non-elastic scattering due to the (n,2n) reaction (σ = 415 mbarn[4]); in principle this reaction may also be considered by nuclear evaporation theory but with two neutrons emitted from the compound nucleus rather than one. However the theory is more complex than for inelastic scattering and values of the numerical constants to adopt in the calculations are more uncertain. For the sake of simplicity therefore we shall treat (n,2n) reactions in the same way as the inelastic scattering, i.e. as though they were isotropic elastic scattering events.

Consequently the differential cross section for a neutron of energy E_n to produce a primary knock on of energy T due to all scattering processes may be written as

$$K(E_n, T) = \frac{4\pi}{T_{max}} k_e(E_n, \cos\theta) + \frac{\sigma_{ne}(E_n)}{T_{max}} \quad \ldots (43)$$

where σ_{ne} is the total non elastic cross section. Fig.8 shows K as a function of T/T_{max} for $E_n = 1$ and 14·1 MeV.

Next we require to calculate N, the number of vacancy-interstitial pairs created by a primary knock on of energy T as it dissipates its energy to the lattice. A number of authors have considered this problem; one of the simplest solutions, due to Kinchin and Pease[6], was described in detail in Section 2.2.2. It may be summarised by stating that for

$$\left.\begin{array}{ll} E_d \leq T \leq 2E_d & N = 1 \\ 2E_d \leq T \leq A & N = \frac{T}{2E_d} \\ T \geq A & N = \frac{A}{2E_d} \end{array}\right\} \quad \ldots (44)$$

where E_d is the energy required to displace an atom and A the atomic weight of the material, expressed in units of keV. In the absence of any known experimental values of E_d for niobium we shall assume it to be the same as for molybdenum, namely 37 eV[32].

The advantage of the Kinchin-Pease approach, which we shall adopt here, is that it is simple to apply to the present problem. However it undoubtedly overestimates the number of defectsproduced at low energies and underestimates the number at high energies. A rather more satisfactory treatment has been given by Lindhard et al[33]. However several of the interesting parameters which are derived below are not dependent on the number of defects formed per primary; furthermore in connection with those parameters which are dependent on this number the general trends and conclusions should not be affected by the Kinchin-Pease approximation.

On the basis of the above assumptions a number of parameters were calculated for $E_n = 1$ and 14·1 MeV and the results presented in Table 5. These parameters are

(a) The average energy of primary knock ons, $\bar{T}$. This is defined as

$$\bar{T} = \frac{\int_0^{T_{max}} T\,K\,dT}{\int_0^{T_{max}} K\,dT} \quad \ldots (45)$$

(b) The cross section for the production of Frenkel (i.e. vacancy-interstitial) pairs, σ_d. This is defined by the relationship

$$\sigma_d = \int_{E_d}^{2E_d} KdT + \frac{1}{2E_d}\int_{2E_d}^{AkeV} TKdT + \frac{A}{2E_d}\int_{AkeV}^{T_{max}} KdT \qquad \ldots (46)$$

As a result the concentration of Frenkel pairs in a material which has been irradiated to a neutron dose φ is simply $\varphi\sigma_d$.

(c) The cross section for the production of primary knock ons which result in the displacement of atoms, σ_s.

$$\sigma_s = \int_{E_d}^{T_{max}} KdT \qquad \ldots (47)$$

(d) The cross section for the production of primary knock ons with an energy greater than 2·5 keV, σ_c i.e.

$$\sigma_c = \int_{2\cdot5\ keV}^{T_{max}} KdT \qquad \ldots (48)$$

This defines the probability of producing a region around the primary knock on with an appreciable number of vacancies. Such vacancy rich regions are believed to harden the material at low temperatures ($\lesssim 700^{o}C$ in niobium, see Section 4.2); they may also act as nuclei for the production of voids. The value of 2·5 keV for the lower limit of the integral in Equation 46 is an approximate figure based on the discussion of Odette[27].

Table 5 shows the numerical values of these parameters for neutron energies of 1 and 14·1 MeV; also shown in the ratio of the 14·1 MeV parameter values over the comparable figures at 1 MeV.

TABLE 5

Values of various damage parameters for neutron energies of 1 and 14·1 MeV

E_n MeV	$\bar{T}$ keV	σ_d ← barns →	σ_s	σ_c
1	13·0	1230	6·78	5·74
14·1	181	3010	3·94	3·80
Ratio	13·8	2·44	0·58	0·66

The noteworthy feature of Table 5 is the comparative insensitivity of the various cross sections with neutron energy. Since the inelastic scattering, which makes a comparatively more important contribution at energies above 1 MeV, has been treated as

though it were elastic the ratio of the $\bar{T}$'s will be too high. However this should be more than compensated by the Kinchin-Pease approximation so that the ratio of the σ_d's is expected to be on the low side. Values of σ_s and σ_c are almost the same as the total cross sections and so should be little affected by the approximations.

Two other independent calculations of σ_d have been performed recently. In the first, by Myers[34], the entire neutron scattering was treated as though it were elastic and isotropic and the formalism of Seitz and Koehler[35] was mainly used to describe the transfer of energy from the primary to the lattice. The other calculation, which must be regarded as the most accurate made so far, is due to Robinson[36]. Neutron elastic scattering was treated in the same manner as by the present author, inelastic scattering by nuclear evaporation theory, and other non-elastic scattering (mainly due to (n ,2n) processes) was treated as though it were inelastic. The slowing down of the primaries was treated by means of the Lindhard theory[33].

In his paper Robinson shows graphically the variation of $\bar{T}$ with E_n for niobium. Reading off the values at 1 and 14·1 MeV from his curve we find that $\bar{T}$ = 12·6 ± ·3 and 106 ± keV respectively. When these figures are compared with the corresponding ones in Table 5 we see that at 1 MeV there is good agreement but that at 14·1 MeV the figure calculated here is considerably higher than Robinson's. Bearing in mind the approximation used in the present treatment these conclusions are what one might expect. It is also of interest to note that Robinson's ratio of the $\bar{T}$'s at these two energies is 8·4 ± ·3.

Robinson and Myers have both calculated the ratio of σ_d's at high and low neutron energy. However the actual values of these energies are slightly different compared with those used here. Robinson considered 15 and 1 MeV neutrons while Myers used 14 and 1·4 MeV. It is unlikely, though, that a neglect of this energy variation will affect the comparison appreciably. The values of these ratios calculated by Robinson and by Myers are 3·91 and 7·8 respectively. Assuming that Robinson's figure is the most accurate one it is understandable from the discussion above why the figure calculated here is on the low side. Presumably Myers' value is on the high side because his most serious approximation is the assumption that all scattering is elastic and isotropic. Bearing in mind that in fact the wall of a fusion reactor will be damaged by a spectrum of neutrons due to back scattering from the blanket it is of interest to quote also Robinson's figures of the σ_d ratios in niobium at 5 and 10 MeV with respect to 1 MeV. These are 2·19 and 3·00 respectively.

In conclusion it would seem appropriate to extend Robinson's calculations to neutron spectra which are typical of fission and fusion reactors in order to obtain an estimate of

the relative damage effectiveness of neutrons in the two types of reactor; such calculations are being performed currently at A.E.R.E. by Dr S. Blow. However reference to the cautionary words at the beginning of Section 4 must be made, for even if this relative damage effectiveness were known with perfect accuracy the radiation damage effects which are likely to be encountered in a fusion reactor could never be predicted with complete certainty from fission reactor irradiations.

4.2 The Effect of Neutron Irradiation on the Yield Stress and Ductility of Niobium

Changes in the mechanical properties of niobium due to neutron irradiation in fission reactors have been reported by a number of authors[37-40]; however this work has been confined entirely to low neutron doses (10^{18} - 2×10^{20} neutrons cm^{-2}) and low irradiation temperatures (16 - 330°C). There is not complete agreement between the results of the different investigations which is not altogether surprising since they are likely to be sensitive to the impurity content of the material (e.g. the yield stress of unirradiated niobium is very sensitive to the oxygen concentration). However the following general conclusions may be made: (a) In all cases an increase in the yield stress of the order of 10,000 psi was observed. (b) The tensile stress also increases but not by so large a value. (c) The temperature dependence of the yield stress is only slightly affected by the irradiation. (d) The ductility is reduced to very low values.

The radiation induced property changes anneal out by 600°C[37], 800°C[39] and between 650 and 1000°C[40]. It is of interest to compare these figures with the prediction[41] that in metals complete recovery should occur by 0·35 T_m, where T_m is the melting point of the material on an absolute scale. For niobium this implies that recovery should be complete at 686°C.

The above discussion might lead one to suppose that provided the containment vessel is maintained at a temperature above, let us say 700°C there should be little change in its mechanical properties as a result of neutron irradiation. However to be sure of the validity of this conclusion some experimental results based on high temperature high dose irradiations are necessary. In the absence of such information on niobium it is perhaps of interest to mention some comparable data relating to an austenitic stainless steel[42]. Irradiation at 538°C (≡ 0·49 T_m) to a dose of $1{\cdot}4 \times 10^{22}$ neutrons cm^{-2} resulted in an appreciable hardening of the material which, from electron microscope observations, was correlated with the formation of Frank sessile loops and voids. To a first approximation these defect aggregates and also the hardening annealed out at about 816°C (≡ 0·65 T_m). It appears therefore that for this particular stainless steel the empirical rule that the

hardening anneals out at a temperature of about 0·35 T_m is only valid for low doses, say less than 10^{20} neutrons cm^{-2}. It remains to be seen whether niobium behaves in a similar manner. If it does then appreciable hardening of the containment vessel is to be expected since for niobium 0·49 T_m corresponds to 1070°C; also the hardening would only anneal at about 1509°C.

4.3 Swelling Caused by Radiation Produced Voids

In Section 3.2.1 we discussed the swelling which was produced by helium bubbles in equilibrium. In the present section we discuss the possibility that swelling may also be caused by void formation. In order to avoid confusion we shall always use the word "bubble" to describe a cavity for which the pressure of the contained gas is either at or approximates to the equilibrium pressure, i.e.

$$p \sim \frac{2\gamma}{r} \pm \sigma \qquad \ldots (49)$$

using the notation of Equation 28. The positive and negative signs refer to compressive and tensile stresses respectively (in many cases of interest σ may be neglected). By contrast we shall use the word "void" to describe a cavity in which the gas pressure is considerably smaller, say by more than an order of magnitude, than this equilibrium pressure.

During the past two or three years it has been shown that above a critical dose and over a specific temperature range, both of which depend on the material, voids are introduced into a number of metals and alloys. Unfortunately no observations on void formation in niobium have been reported so far, though it is understood that appropriate samples for such an investigation are being irradiated currently at Dounreay (Mosedale, private communication). We shall therefore present a survey of the work performed on other materials in an attempt to predict the conditions required for void formation in niobium, the magnitude of the swelling and the temperature at which voids can be eliminated following the irradiation. However it is pertinent to point out at the outset that it has not yet been established conclusively that appropriate experimental conditions exist for voids to be formed in all metals and alloys. Furthermore these conditions may mean that for certain materials void production may be completely neglected in practice (e.g. if the critical dose for void formation is 10^{24} neutrons cm^{-2} or greater).

It is difficult to define precisely the dependence of swelling on the irradiation temperature and neutron dose owing to the scatter in the experimental results. However it does appear that for a specific dose the swelling goes through a maximum within the temperature range over which voids are formed; also at a constant temperature results to date indicate that to a first approximation the swelling is proportional to the dose.

Table 6 summarises some of the results which have been obtained on voids; it represents by no means a complete survey of the literature but rather a selection which enables the swelling of a number of different materials to be compared. The irradiation and annealing temperatures in this table are expressed both in ^{o}C and as a fraction of the material's absolute melting point.

TABLE 6

Swelling due to voids in a number of materials

Material	Neutron Dose neutrons cm^{-2}	Irradiation Temperature ^{o}C and fraction of T_m	Fractional volume change $\times 10^{-3}$	Annealing Temperature ^{o}C and fraction of T_m	Reference Number
V	$1{\cdot}7 \times 10^{22}$	630(·46)	3·7	750–850 (·52–·57)	43
V–20% Ti	5×10^{22}	375–475 (·33–·38)	0		44
Ni	5×10^{19}	380(·38)	1·1	600–800 (·51–·62)	45,46
	$1{\cdot}2 \times 10^{20}$	260(·31)	3		
Cu	$1{\cdot}2 \times 10^{20}$	260(·39)	3		45
"Pure" Al	$3{\cdot}5 \times 10^{20}$	50(·35)	< 4	250–300 (·56–·62)	47
"Commercial" Al	$1{\cdot}5 \times 10^{22}$	50(·35)	15	230–315 (·54–·63)	47,48
Type 316 stainless Steel		≤ 380(·39)	0	700–900 (·58–·70)	49
	$5{\cdot}2 \times 10^{22}$	450(·43)	8		
	$7{\cdot}8 \times 10^{22}$	500(·46)	70		
	$3{\cdot}2 \times 10^{22}$	560(·50)	2		
	Accelerator irradiation			< 800(·64)	50
Type 304L stainless steel	9×10^{21}	373–463 (·39–·44)	1		51
	6×10^{22}		10		

Table 6 suggests that to a first approximation the temperature ranges for the formation and annealing of voids are comparable in different materials provided temperatures are expressed as a fraction of the melting point. It also suggests that voids are formed in the temperature range $\cdot 31–\cdot 50T_m$ (though most results occur in the range $\cdot 38–\cdot 46T_m$) and annealing takes place in the range $\cdot 51–\cdot 70T_m$ (though it would not conclusively violate any of the results if the range was reduced to $\cdot 51–\cdot 64T_m$).

It is evident from Table 6 that the resistance to swelling various considerably from material to material; for example for a specific neutron dose much larger swellings may be encountered in nickel than in stainless steel. The reason for this appreciable variation between materials is not properly understood at present although some clues are now

emerging. For example it has been found that the swelling associated with voids, due to radiation damage by energetic ions, is considerably enhanced if helium atoms have previously been injected into the material[50]. It seems reasonable to suppose therefore that gas atoms, either already present in the material or produced as a result of nuclear transmutation reactions, are required for the formation of void nuclei. The critical flux for void formation may thus be determined by the overall concentration of gas produced, and also by the number of gas atoms required to form each nucleus. Presumably this latter quantity depends on the difference between the formation energies of a void nucleus and that of other vacancy aggregate embryos (e.g. planar defects).

Another parameter which appears to affect the swelling is the purity of the material. Thus Table 6 suggests that less pure materials and alloys may be more resistant to swelling than pure metals; for example voids were observed after a dose of $3{\cdot}5 \times 10^{20}$ neutrons cm^{-2} in pure aluminium but not in a commercial grade of the same material[47]. It was suggested that this difference could be due to impurities in the commercial grade material "gettering" the gaseous impurities from the bulk of the material and so preventing void nucleation.

The factors discussed so far appear to affect the swelling through changing the ease by which void embryos may be nucleated. However the magnitude of the swelling is also affected by the extent to which voids grow. It must be remembered that radiation damage produces an equal number of vacancies and interstitials; as a result if the capture cross section of the various sinks in the crystal (including the void embryos) were equal for both interstitials and vacancies, voids in general would not grow and the swelling would not be approximately proportional to the dose. Electron microscope observations suggest that the interstitials condense into planar defects such as faulted loops, so one possibility is that the strain field around such defects attracts preferentially migrating interstitial atoms (because of the much smaller strain fields around voids any corresponding preferential attraction near voids could well be less important). The extent by which these faulted loops and other defects are preferential sinks for interstitials rather than vacancies, which will clearly affect the magnitude of the swelling, will obviously depend on the nature of the material. Unfortunately our present state of knowledge concerning this effect does not enable any quantitative comparisons between different materials to be made.

Let us now attempt to make some predictions about the swelling due to void formation in niobium on the basis of the above discussion. If voids are formed over the irradiation temperature range $\cdot 31 - \cdot 50\ T_m$ this corresponds to 577-1098°C; on the other hand if we assume the smaller range $\cdot 38 - \cdot 46\ T_m$ the temperatures are 769-988°C.

In order to assess the magnitude of the swelling let us assume that it is comparable to either vanadium or stainless steel. If the swelling is proportional to dose then for $2{\cdot}33 \times 10^{23}$ neutrons cm^{-2} the swelling by analogy to vanadium and stainless steel is approximately 5·1 and 21% respectively; the latter figure was derived from the most pessimistic experimental value for stainless steel given in Table 6. Note that we have neglected the higher neutron energies encountered in fusion reactors; as a result these estimates may be on the low side since with higher neutron energies more gas atoms are formed and also more atoms are displaced per incident neutron. On the other hand the large impurity concentrations introduced at high energies (see Table 1) may help to decrease the swelling. It appears therefore that a swelling of the order of 10% due to void formation may be predicted tentatively; clearly some experimental figures are required. Finally it may be noted that no information is currently available on the effect of stress on the swelling.

If voids in niobium anneal over the temperature range $\cdot 51-\cdot 70\ T_m$ this corresponds to 1125-1646°C; on the other hand if we assume the smaller range $\cdot 51-\cdot 64\ T_m$ the temperatures are 1125-1481°C.

In conclusion it appears likely that at wall temperatures which are dictated by other considerations, voids will be formed in the containment vessel. Perhaps the associated swelling may be relieved by periodic annealing; however during such anneals the swelling may be made even worse due to the helium forming large bubbles (Section 3.2). Fortunately there is every prospect that within the next few years some rather clearer conclusions than those given here will be possible in view of the very large effort currently being put into the subject of voids by laboratories concerned with the design of fast fission reactors.

4.4 The Enhancement of Creep by Neutron Irradiation

We shall introduce the present topic by making a few general comments on creep rates in unirradiated niobium. No attempt to review the subject of creep will be made here since many authors have done this in the past. (For a recent account see Ref.52).

Since the deformation due to creep of the containment vessel should not exceed of the order 1% after 20 years, experiments which measure creep rates of the order 10^{-7} per hour are of interest here; in addition for such long times we are principally concerned with steady-state or secondary creep. Not surprisingly technical reasons demand that experiments are normally performed for shorter times and at higher strain rates, say 10^{-5} - 10^{-3} per hour. A number of such experiments have been performed on niobium[53-57]. The correlation of these results is difficult since creep depends on a number of factors including

applied stress, temperature and sample purity. However it appears that to an order of magnitude and for reasonably pure niobium the strain rate at 1000°C is $\sim 5 \times 10^{-5}$ per hour for a stress of 1000 psi. Moreover these results suggest that the creep rate may be decreased by an order of magnitude fairly readily by adding impurities. Further research designed to fabricate a more creep resistant material may possibly decrease the creep rate by an additional order of magnitude. As a result we may infer that at 1000°C the containment vessel can sustain stresses of up to about 500 psi for deformations of up to 1% after 20 years. Note however that this conclusion depends on at least three assumptions: (a) high creep rate data may be applied directly to low creep rates which are of interest here (b) steady state creep has been attained in these experiments so that creep rates will continue unchanged for very long times (c) the creep rate is proportional to σ^n where σ is applied stress and n is about 3-4.

Since creep rates are normally quite temperature dependent we would expect the creep resistance to be significantly lower at 1200°C than at 1000°C. By contrast steady state creep, which is believed to be controlled by diffusion processes, becomes extremely small below about 0·4 T_m. Since for niobium this corresponds to 823°C it is apparent that considerably larger stresses than that indicated above are permissible over the temperature range 600-800°C. This conclusion is in accord with Tottle's data[53] which shows that at 600 and 700°C and for 7000 and 4000 psi respectively primary creep is occurring predominantly, i.e. the creep rate is decreasing monotonically with time so that after 1000 hours it has dropped to the order of 10^{-6} per hour.

Unfortunately the extension of these conclusions to include the effect of irradiation on the creep of niobium is extremely difficult. This is because no in-pile creep measurements have been performed to date on niobium, to the author's knowledge, and also in the absence of a satisfactory theory of radiation enhanced creep, predictions are somewhat hazardous.

A number of attempts have been made to account for the enhancement of the steady-state creep of cubic non-fissile metals by neutron irradiation. For example the suggestion by Shoek[58], that there is an enhancement of the normal diffusion creep by vacancies because of the radiation enhanced vacancy concentration, has been disproved for conditions under which equal concentrations of vancancies and interstitials are present by Mosedale[59]. Hesketh[60] has extended this conclusion to show that quite generally no radiation enhanced creep is possible when creep is governed by diffusion processes such as Nabarro-Herring creep or the climb of edge dislocations. However Buckley has pointed out in a review of

the subject[61] that this assumes that dislocations are unable to slip following climb. If dislocations can climb past barriers and then slip an enhancement of the creep rate due to irradiation will be observed provided that the concentrations of mobile vacancies and interstitials produced by the irradiation are different. This will be the case if, for example, immobile vacancy clusters are formed as a result of the irradiation.

The above discussion has ignored variations in the temperature of irradiation. Billington and Crawford[62] suggested that the enhancement of creep due to irradiation will be a maximum at about 0·5 T_m, which in niobium corresponds to 1097°C. At more elevated temperatures radiation effects should be less pronounced since the concentration of point defects present in equilirbium (which are virtually all vacancies) will then be greater than that produced by irradiation. The results of Appendix 3 in fact confirm that this situation occurs above about 1000°C. On the other hand at lower temperatures the enhanced point defect concentration will be offset by radiation hardening due to point defect clusters which are formed from the displacement damage (see Section 4.2), and also due to the zirconium atoms and helium bubbles produced by the transmutation reactions (Section 2.2.1). In other words at low temperatures radiation enhances both the rate at which dislocations can climb over obstacles and the number of obstacles in the solid. Of course the transmutation products (which Billington and Crawford ignored since they were concerned with fission reactor irradiations) should also make a contribution to the hardening at higher temperatures. As a result the difference in the radiation enhanced creep on going from a fission to a fusion reactor will not be due simply to differences in the overall neutron flux and the energy spectrum of primary knock-ons.

In conclusion therefore it is very difficult to make any definite predictions concerning the effect of neutron irradiation on the creep rate of the containment vessel. In the light of the above discussion it is not impossible that creep rates may be little affected under the conditions which are of present interest, but clearly some experimental data, preferably coupled with a greater understanding of the subject, is required before any firmer conclusions may be drawn.

4.5 The Effect of Radiation on the Thermal Conductivity of Niobium

In general, provided irradiations are carried out at room temperature or above, displacement damage produces negligible changes in the thermal conductivity of metals[62]. Although no specific measurements on neutron irradiated niobium are known there is no reason to doubt thatthis general conclusion applies to this material also.

Presumably the formation of bubbles and voids by irradiation will produce small changes in the thermal conductivity. However since other considerations preclude the possibility that the volume fraction of these aggregates may be greater than a few per cent, we would not expect the fractional change in the thermal conductivity to be appreciably greater than this figure.

Changes in the thermal conductivity will also occur as a result of the transmutation of up to 10% of the atoms to zirconium (Table 1). So far as is known the thermal conductivity of such alloys at high temperatures has not been reported. However in view of the similarity in the physical properties of the two constituent elements[9,63] and the fact that a solid solution is formed over the whole composition range it seems reasonable to assume that the thermal conductivity is not affected markedly by the alloying (say by more than about 10%).

We conclude therefore that changes in the thermal conductivity due to irradiation will not seriously affect the conduction of heat across the wall of the containment vessel.

5. RADIATION EFFECTS RELATING TO THE INNER SURFACE OF THE CONTAINMENT VESSEL

In this section we shall consider the ejection of atoms from the inner surface of the containment vessel due to neutron bombardment; this will result in the erosion of the vessel and contamination of the plasma. Two possible ways by which this can occur are sputtering and the evaporation of atoms from thermal spikes located close to the surface; these are discussed in Sections 5.1 and 5.2 respectively. Note that in accordance with the basic assumptions made in Section 2.1 we shall only consider the ejection of atoms due to neutron irradiation; in particular the sputtering of materials by energetic ions, a subject which has received considerable attention, will be omitted.

5.1 The Sputtering of Niobium by 14·1 MeV Neutrons

Very few measurements of the 14·1 MeV neutron sputtering ratio have been reported. Keller[65] was unable to measure any sputtering from Au, W, Cu, and In and so put an upper limit to the sputtering ratio which varied between 4×10^{-2} and 6×10^{-4}, depending on the metal. For molybdenum, which should be similar to niobium, he suggested on the basis of these measurements a corresponding upper limit of 10^{-4} and also calculated an actual value of 10^{-6} based on the theory of Almen and Bruce[66]. The only other known experimental neutron sputtering ratio is 3×10^{-3} for gold by some Russion workers[67].

It appears likely therefore from the rather limited evidence which is available that neutron sputtering will not produce any serious contamination of the plasma or erosion of the vessel.

5.2 Contamination Due to the Evaporation of Atoms from Thermal Spikes

It was pointed out in Section 2.2.2 that atoms which receive energy as a result of neutron collisions will subsequently share this energy with the surrounding atoms by means of a collision cascade. This results in an approximately spherical region around each primary knock-on being raised to a high temperature in a time of the order of 10^{-13} secs; these regions, which are known as thermal spikes, will then lose their energy by means of thermal conduction in a comparatively much longer time.

When thermal spikes occur close to the inner surface of the wall atoms on the surface will be raised to high temperatures and as a result a fraction of them will be evaporated. Let us now calculate how much the plasma is contaminated as a result of this evaporation.

The evaporation of atoms from thermal spikes has been measured by Thompson, Nelson and Sheldon[68,69]. Integrating Equation 9 of reference 68 over the energy of the emitted atoms we find that the total number of atoms evaporated per unit area per unit time, Φ, is given by

$$\Phi = \left(\frac{8kT}{\pi M}\right)^{\frac{1}{2}} N\, e^{-E_b/kT} \qquad \ldots (50)$$

where T is the temperature of the surface, N the number of atoms per unitvolume, M their mass and E_b the binding (or sublimation) energy of atoms on the surface. (Note that Equation 9 of reference 68 possesses a typographical error in that a factor E has been omitted). Equation 50 assumes that the statistical variation in energy obeys a Maxwell-Boltzmann distribution, which should be valid for energy values of concern here, namely above E_b.

Let us assume that the radius, r, of all thermal spikes is the same and that only primaries which occur at depths up to a distance r from the surface will heat surface atoms. Then to a good approximation the number of primaries which will produce surface heating per unit area of the vessel in unit time will be $N\sigma r\varphi$, where σ is the neutron collision cross section and φ the neutron flux. For the sake of simplicity let us further assume that all of these spikes intersect an area πr^2 at the surface and that the temperature-time relationship of the spike is a step frunction, being at $T\ ^{o}K$ for a time τ and at room temperature at all subsequent times. (In view of the exponential dependence of Φ on temperature this latter assumption is not so drastic as might appear at first sight). If A is the surface area of the vessel, V the volume of the plasma, n_p the ion density in the plasma then the fractional contamination rate of the plasma per unit time is

$$\frac{d}{dt}\left(\frac{n_i}{n_p}\right) = \frac{\pi N^2 r^3 \sigma \tau \varphi A}{n_p V}\left(\frac{8kT}{\pi M}\right)^{\frac{1}{2}} e^{-E_b/kT} . \quad \ldots (51)$$

T and r are related to the energy E available from the primary to heat the atoms by the relationship

$$T = T_o + \frac{E}{2\pi r^3 Nk} \quad \ldots (52)$$

where T_o is the ambient temperature of the wall. We saw in Section 4.1 that primary knock-ons will receive energy in the approximate range 0-600 keV but that a maximum of only about 100 keV is transferred to the surrounding atoms, so producing a temperature rise. However let us deliberately overestimate the contamination rate by assuming that every primary receives an energy of 575 keV and all this energy is used to heat the surrounding lattice. Since Φ increases rapidly with T we expect therefore that the contamination rate will be overestimated by several orders of magnitude. Also we shall overestimate this rate further by assuming a high value for τ, based on the experimental data[68,69], namely 10^{-11} sec. Values taken for those constants which have not been given previously were $T_o = 600^oC$ and $E_b = 6{\cdot}79$ eV. The resulting contamination rate calculated from this data is about 10^{-5} per second; however since this calculated value must be at least two orders of magnitude too high we may conclude that under all realistic situations the contamination and erosion due to evaporation from thermal spikes may be neglected.

6. CONCLUDING REMARKS

In this section we shall summarise the principal results of this study, point out some of its limitations and shortcomings and indicate some experiments by which it is hoped they may be overcome.

6.1 A Summary of the Principal Results of this Study

In the interest of brevity the conclusions enumerated here have sometimes been simplified and over-stated. Therefore before applying any of the assertions found in this section the reader is strongly advised to read the detailed discussion in the appropriate section which is quoted after each conclusion.

1. In a proposed model of an economic reactor[1] doses of typically $3{\cdot}7 \times 10^{14}$ $cm^{-2}sec^{-1}$ of 14·1 MeV neutrons are incident on the containment vessel, corresponding to a total dose of $2{\cdot}3 \times 10^{23}$ cm^{-2} after 20 years; these fluxes neglect neutron back scattering from the surrounding structure (Section 2.1).

2. The containment vessel is assumed to be fabricated of niobium which will operate in the temperature range 600-1200°C (Section 2.1).

3. Nuclear reactions between 14·1 MeV neutrons and the niobium atoms result in the production of approximately 10, 0·5 and 0·275 atomic per cent of zirconium, hydrogen and helium respectively after 20 years. The zirconium will form a solid solution with niobium, hydrogen will rapidly diffuse out of the material while the helium will aggregate into a number of comparatively immobile bubbles (Sections 2.2.1, 3.1 and 3.2).

4. Helium bubbles will result in a swelling of the containment vessel, the magnitude of which increases with the bubble size. If all the bubbles have a radius of 10^{-5} cm the fractional swelling after a 20 year irradiation is about 6% (Section 3.2.1).

5. If bubbles are produced by the coalescence of randomly migrating helium atoms to form immobile pairs which subsequently grow into (immobile) bubbles, then the swelling after a 20 year irradiation is equal to or less than 1%, the exact value depending on the irradiation temperature (Section 3.2.2.1).

6. In general bubbles will not be immobile since niobium atoms can migrate along their surface. Three possible mechanisms considered here by which bubbles may move are Brownian motion, temperature gradients and stress gradients (Section 3.2.2.2 and Appendix 4).

7. The motion of bubbles due to Brownian motion generally modifies only slightly the swelling, as calculated by the simple homogeneous nucleation model (Section 3.2.2.2).

8. In contrast temperature gradients within the wall will enhance the swelling so that at irradiation temperatures of 1000 and 1200°C its magnitude will be 3 and 30% respectively. However at 600°C the enhancement will be insignificant. It turns out that the swelling obtained in practice will be governed by the temperature gradient (Section 3.2.2.3).

9. Stress gradients in the wall will affect its swelling negligibly (Section 3.2.2.4).

10. In principle, application of a hydrostatic stress is capable of reducing significantly the magnitude of the swelling (Section 3.2.3).

11. The results of the swelling calculations are little affected when allowance is made for the impurities, dislocations and grain boundaries which will be present in the material (Section 3.2.4).

12. The re-solution of gas atoms in bubbles back into the lattice due to irradiation may be neglected (Section 3.2.5).

13. Under tensile stresses bubbles can in principle grow indefinitely and so produce fracture when they join together. However in practice fracture of the containment vessel within the reactor's lifetime seems unlikely to be a limiting factor (Section 3.2.6).

14. 14·1 MeV neutrons will also collide with lattice atoms and so transfer kinetic energy to them. The energy given to these primary knock ons is dissipated by means of

collision cascades with the surrounding lattice, resulting in ionisation and the production of point defects. These point defects will modify the physical properties of the containment vessel (Section 2.2.2).

15. The ratios of the cross sections at a neutron energy of 14·1 MeV compared with 1 MeV for the production of primary knock ons and point defects are about 0·6 and 2·4 respectively, i.e. these ratios are not a very sensitive function of the neutron energy (Section 4.1).

16. Neutron irradiation generally increases the hardness and lowers the ductility of materials. However on the basis of low dose measurements these effects will not occur at irradiation temperatures of interest here. It remains to be seen whether this is also valid in niobium at high doses - results on stainless steel indicate differences between low and high doses (Section 4.2).

17. Large swellings may occur as a result of void formation since calculations indicate that voids are formed at temperatures of irradiation in the range 577-1098^{o}C and disappear above about 1125^{o}C. Swellings of the order of 10% are possible (Section 4.3).

18. In the light of our present knowledge it is very difficult to make any quantitative predictions on the enhancement of the creep rate by irradiation. It may well be that over certain ranges of interest here this enhancement is negligible (Section 4.4).

19. Radiation effects, due to both displacement damage and transmutation reactions, will produce only unimportant changes, from a practical point of view, in the thermal conductivity of the wall (Section 4.5).

20. Neutron irradiation can result in the loss of niobium atoms from the wall into the plasma by sputtering and thermal evaporation. However this loss rate is insufficient to contaminate the plasma seriously or to cause appreciable erosion of the wall (Section 5).

6.2 Some Limiations of the Present Work

It is inevitable that a study of the present nature should possess a number of inherently unsatisfying features owing to the need to simplify a complex system comprising of a number of different types of defect and also because of at least a partial ignorance of how these defects behave. A number of assumptions and simplifications which were made in the calculations have already been given in the appropriate sections; here we shall list only some of the major shortcomings of the whole study.

1. Throughout this study we have assumed that the 14·1 MeV neutrons produced in the plasma pass through the wall once and are then absorbed in the blanket. In practice of course neutrons will be back-scattered, so that the wall is irradiated with an additional spectrum of neutrons possessing energies up to 14·1 MeV. This implies that the transmutation

reactions and displacement damage have been underestimated in the present study. From neutronics calculations on a number of blanket configurations Blow et al[70] have reported a neutron spectrum in the wall, while Steiner[71] has quoted helium and hydrogen accumulation and atom displacement rates. It appears from Steiner's work that the helium and hydrogen production rates may be enhanced by round about factors of 2 and 3 respectively as a result of including neutrons which have been scattered back into the wall. Unfortunately since the method of calculating the displacement rate was not indicated it is difficult to estimate the corresponding enhancement factor.

2. All the calculations have assumed that the vessel consists of pure niobium. However since about 0·5% of the material is transformed into zirconium per year some modifications to the calculated results may be expected. For example some of the values of the constants assumed in the calculations may be time-dependent; nevertheless although numerical results may be affected the general trends and dependence on the various parameters should not normally be seriously affected.

One way by which the results could be modified is through the trapping (possibly only temporarily) of point defects and helium atoms by zirconium as they migrate towards voids and bubbles respectively.

3. All the calculations on helium bubbles have assumed a time-independent helium atom concentration, corresponding to that occurring after 20 years. As a result the conclusions will tend to err on the pessimistic side (however this will be at least partially compensated by item 1 above).

4. In Sections 3.2 and 4.3 various effects resulting respectively from the presence of equilibrium bubbles and voids were discussed as though these were two completely different and independent types of defect. In practice it seems possible that gas contained spherical cavities which are neither exactly bubble or void like may be formed, but unfortunately it is not possible to make any more definite conclusions; in the absence of a satisfactory understanding of this subject therefore it was inevitable that the best that could be done was to consider these two particular possibilities separately.

In recent years voids in reactor irradiated materials have been studied extensively. On the basis of this work it might be expected therefore that in the wall of a fusion reactor all cavities containing gas will be void-like since an enhanced concentration of vacancies will be present as a result of the displacement damage. However before arriving at this conclusion several points must be borne in mind: (a) void growth is dependent on the excess concentration of vacancies, compared with interstitials, which may migrate to cavities, but at present it is not possible to calculate this excess with any certainty.

(b) The number of vacancies required by a bubble for each helium atom added increases with radius if the bubble is to remain in equilibrium (Table 7). Since the helium production rate remains approximately constant with time cavities will tend not to be void-like when their radii are greater than some critical value, which at present cannot be calculated since the excess vacancy concentration is not known. (c) Bubbles are more likely to occur in a thermonculear than in a fission reactor since the helium production rate per incident neutron is considerably greater at 14·1 MeV compared with 1 MeV. (While it is true that the atom displacement rate is also enhanced at 14·1 MeV this should not be as great as the enhancement of the helium production rate). Consequently if voids rather than bubbles are observed in niobium after irradiation in a fast reactor it is by no means certain that the same result would be obtained in a fusion reactor.

5. The values of many of the constants used in Section 3.2 are not known with any precision, and in particular D, the diffusion coefficient of helium in niobium, D_s and D_{gb}, the coefficients for self diffusion on a gas/solid interface and a grain boundary respectively and Q_s^*, the heat of transport for surface diffusion. However it seems likely that while numerical results will be altered when better values of these constants are known the general conclusions and trends arrived at here will not be modified significantly.

6. All the radiation damage effects predicted in Section 4 are of necessity based on irradiations in fission reactors. It is quite possible that the increased mean energy of primary knock-ons and also the enhanced gas production in a fusion reactor will modify these conclusions.

6.3 Some Experiments Which May Help in Further Assessing the Radiation Damage in the Containment Vessel

Clearly ideal radiation damage experiments would employ a high intensity source of 14·1 MeV neutrons. Although none have been built so far it is perhaps relevant to point out that Lidsky and Colombant[72] have suggested that by the use of a windowless gas target a 14·1 MeV source producing 10^{15} neutrons sec^{-1} in a volume of 1 cm^3 could be built. On this basis thin foils and bulk samples could possibly be irradiated at dose rates of $\sim 10^{14}$ and 10^{13} neutrons cm^{-2} sec^{-1} respectively. They estimated that the capital cost would be £3 million and the annual running cost (mainly due to tritium) £1 million.

In the absence at present of such sources we must consider other means of producing radiation damage and discuss their respective merits and limitations. There are at least three basic types of machine which may be used singly or in combination to produce radiation damage, namely reactors, accelerators producing a variety of ions, and high voltage

electron microscopes operating above approximately 800 keV.

Fission reactors generally suffer from the disadvantage of not producing high enough neutron doses, since fluxes greater than about 5×10^{15} neutrons cm^{-2} sec^{-1} are required if samples are to be irradiated within a convenient time to doses comparable to those encountered by the wall during the lifetime of a thermonuclear reactor; another disadvantage of fission reactors is that neutron energies are lower than in fusion reactors. On the other hand the distribution of energy in the primary knock ons is more comparable to that in a fusion reactor than is the case for ion and electron irradiations; also because neutrons penetrate large distances into matter neutron irradiations alone enable many of the physical property changes which are of direct interest to be measured directly while ion and electron irradiation effects can be studied in general only in the electron microscope. On the other hand both accelerator and high voltage electron microscope irradiations can produce displacement rates comparable to and higher than that encountered in a fusion reactor. Furthermore accelerators are extremely versatile machines; in principle one can vary readily the nature of the ion, its energy and the current density. Also during the irradiation the sample may be observed continuously in an electron microscope under controlled temperature conditions.

The following is a list of some of the possible irradiations which could be usefully performed with these three types of machine:

1. High dose neutron irradiation of niobium in a fast reactor.

2. Neutron irradiation of boron doped niobium. The advantage of using such material is that irradiation will produce displaced atoms and helium simultaneously by means of fast and thermal neutrons respectively. The accompanying disadvantage is that lithium atoms are also produced and these may affect the results.

3. Accelerator irradiations to produce displaced atoms. By using thin foils and sufficiently high accelerating energies most of the ions can be made to pass through the foil, thus reducing contamination by the impurity ions. However under these circumstances the defect concentration will be less since diplacement rates increase towards the end of the ion's path. In fact high dose rates without contamination are possible if niobium ions are used to create the damage. In particular with 300 keV niobium ions we can simulate to a first approximation the primary knock ons which are produced by 14·1 MeV neutron irradiations. Finally as a general word of caution some check should be made in very high dose accelerator irradiations that the damaged region it is desired to create is not sputtered off by the incident ions.

4. Electron irradiations of niobium in a high voltage microscope.

5. Similar experiments to those in items 1, 3 and 4 above except that the niobium is pre-loaded with helium atoms by means of an α particle irradiation. By suitable heat treatment this helium could either be dispersed atomically or aggregated in the form of bubbles before initiating the displacement damage. Such experiments would be of help in determining whether as a result of displacement damage single helium atoms agglomerate into bubbles or become the nuclei for void formation, and also whether the damage is capable of re-dissolving helium bubbles.

6. Experiments identical to those in items 1-5 above except that the starting material is an alloy of niobium containing up to 10% zirconium.

Naturally a range of irradiation temperatures would be desirable in all these experiments.

Most samples which have undergone charged particle displacement damage will inevitably be studied under an electron micrscope (operating either at high or conventional ($\sim$ 100 keV) voltages). After neutron irradiation measurements of macroscopic physical properties such as changes in volume and mechanical properties are also possible. In addition measurements in pile of properties such as creep may be possible.

It would also be of interest to check some of the predictions concerning mean bubble sizes which were made in Section 3.2.2. For example by inplanting niobium foils at low temperatures with α particles from a cyclotron and annealing at higher temperatures aggregation due to Brownian motion could be studied. In addition temperature and stress gradients could be applied during anneals to check the predictions of Sections 3.2.2.3 and 3.2.2.4.

7. ACKNOWLEDGEMENTS

I would like to acknowledge the interest shown in this work and help given by many colleagues at Harwell and Culham and in particular the many illuminating discussions I have enjoyed with Mr J.T.D. Mitchell.

APPENDIX 1

THE MAINTENANCE OF EQUILIBRIUM BY BUBBLES DURING THEIR GROWTH

We have seen in Section 3.2 that bubbles will tend to grow as a result of helium atoms, which are formed in the lattice and which can diffuse, being attached to them. However if during this growth process bubbles are to be maintained in equilibrium vacancies must be added concurrently, the number being dependent on the instantaneous bubble radius.

Assuming that the helium contained in bubbles obeys the perfect gas law we have

$$\frac{8}{3}\pi r^2\gamma = nkT \qquad \ldots (53)$$

from Equations 7 and 8. If as a result of attaching dn helium atoms the bubble expands by an amount dr in order to maintain equilibrium the number of vacancies dH which must be added is

$$dH = \left(\frac{4\pi r^2}{\Omega}\frac{dr}{dn} - 1\right) dn \qquad \ldots (54)$$

Differentiating Equation 53 we have

$$\frac{dr}{dn} = \frac{r}{2n} \qquad \ldots (55)$$

Finally from Equations 53-55 we find that the number of vacancies to be attached per helium atom if the bubble is to remain in equilibrium is

$$\frac{dH}{dn} = \frac{3kTr}{4\gamma\Omega} - 1 \qquad \ldots (56)$$

For bubble radii smaller than 10^{-5} cm, when the perfect gas law is a poor representation of the equation state (Appendix 2), Van der Waals equation was employed in order to calculate the results discussed below. The derivation of the corresponding equation for $\frac{dH}{dn}$ is not given here since in principle it is the same as that given above only mathematically more complicated.

The second column of Table 7 shows $\frac{dH}{dn}$ for different bubble sizes. The third column shows the number of helium atoms being attached to each bubble per second assuming a uniform distribution of identical bubbles, an overall helium concentration of $2{\cdot}75 \times 10^{-3}$ and a helium production rate of $4{\cdot}35 \times 10^{-12}$ helium atoms/atomic site per second. The fourth column, which is obtained by multiplying together the figures of columns 2 and 3 gives the number of vacancies which must be added to a bubble per second if equilibrium is to be maintained.

TABLE 7

The number of vacancies required to maintain a growing bubble in equilibrium

Bubble radius cm	No. of vacancies required per He atom added	No. of He atoms added per second	No. of vacancies required to be added per second
10^{-7}	2	$1{\cdot}6 \times 10^{-7}$	$3{\cdot}2 \times 10^{-7}$
10^{-6}	5	$7{\cdot}9 \times 10^{-5}$	$4{\cdot}0 \times 10^{-4}$
10^{-5}	34	$1{\cdot}6 \times 10^{-2}$	$5{\cdot}4 \times 10^{-1}$
10^{-4}	350	1·6	$5{\cdot}4 \times 10^{2}$
10^{-3}	3,500	$1{\cdot}6 \times 10^{2}$	$5{\cdot}6 \times 10^{5}$

It is evident that the number of vacancies required increases with bubble size; as a result bubbles with radii greater than a certain value will deviate from equilibrium by significant amounts. An attempt to estimate this critical size will now be made.

Unfortunately it is impossible to estimate how radiation affects the net arrival rate of point defects to bubbles without some knowledge of the preferential nature of the various sinks in the lattice for vacancies compared with interstitials. For example if all sinks have an equal probability of absorbing both types the net numbers of vacancies reaching bubbles will be unaffected by radiation since the number of radiation-produced vacancies and interstitials are idential. However the observation of voids in materials after high dose irradiations suggests that, under certain circumstances at least, interstitials are annihilated preferentially by the sinks. It is possible therefore that in situations which are of interest to us the radiation is able to enhance the net vacancy flow to bubbles.

In the absence of any quantitative information on this subject let us assume that we can neglect the effect of radiation on bubble growth and then enquire whether to a reasonable approximation bubbles can remain in equilibrium by means of the vacancies which are present in thermodynamic equilibrium.

First of all let us suppose that bubbles are always in equilibrium. If the gas in bubbles obeys the perfect gas law we may rewrite Equation 53 as

$$\frac{8}{3}\pi r_o^2 \gamma = nkT \qquad \ldots (57)$$

where r has been replaced by r_o the emphasise that this relates to an equilibrium radius. The growth rate of this equilibrium bubble is thus

$$\frac{dr_o}{dt} = \frac{3kT}{16\pi r_o \gamma} \frac{dn}{dt} \qquad \ldots (58)$$

Now if we assume that bubbles nucleate and grow in accordance with the homogeneous nucleation theory of Section 3.2.2.1 and using the notation of that section it follows that

$$\frac{dn}{dt} = \frac{4\pi r_1^3 G}{3\Omega} \qquad \ldots (59)$$

Hence

$$\frac{dr_o}{dt} = \frac{Gr_1^3 kT}{4r_o\gamma\Omega} \qquad \ldots (60)$$

However since in practice the driving force which governs the flow of vacancies to the bubble is its deviation from equilibrium the actual bubble radius r will always be less than r_o and its growth rate will be given by Equation 10 of Reference 15:

$$\frac{dr}{dt} = \frac{D(p - 2\gamma/r)\Omega}{rkT} \qquad \ldots (61)$$

where D is the bulk self-diffusion coefficient. Now since

$$\frac{4}{3}\pi r^3 p = nkT$$

$$p - \frac{2\gamma}{r} = \frac{2\gamma}{r}\left(\frac{r_o^2}{r^2} - 1\right).$$

using Equation 57.

Let us now make the assumption that it is permissible to describe a bubble as being approximately in equilibrium if

$$1 < \frac{r_o}{r} \leqslant 1{\cdot}1$$

If we assume the equality sign to be valid we have

$$p - \frac{2\gamma}{r} = \frac{0{\cdot}462\gamma}{r_o}$$

and Equation 61 now reads

$$\frac{dr}{dt} = \frac{0{\cdot}5\ D\gamma\Omega}{r_o^2 kT} \qquad \ldots (62)$$

If as the bubble grows r is never to deviate from r_o by more than 10% $\frac{dr}{dt} \gtrsim \frac{dr_o}{dt}$. By putting $\frac{dr}{dt} = \frac{dr_o}{dt}$ we can equate Equations 60 and 62 to give the limiting radius r^{lim}.

$$r^{lim} = \frac{2D\gamma^2\Omega^2}{k^2T^2Gr_1^3} \qquad \ldots (63)$$

For radii smaller than this limit $\frac{dr}{dt} > \frac{dr_o}{dt}$ so that the deviation of the bubble radius from the equilibrium value becomes less than 10%.

At 1000^oC with D assumed equal to $4{\cdot}6 \times 10^{-17}$ cm^2 sec^{-1} (11) $r^{lim} \sim 0{\cdot}5$ cm. Since the limiting radius increases with temperature this shows that in the temperature region

1000-1200^{o}C bubbles of all realistic sizes are nearly in equilibrium. However at 600^{o}C, assuming $D = 1{\cdot}4 \times 10^{-24}$ cm^2 sec^{-1} $r^{lim} \simeq 3 \times 10^{-7}$ cm, so that at this temperature bubbles whose sizes are of interest to us here are far from equilibrium.

A rough estimate of the temperature above which bubbles of sizes which are of interest to us are in equilibrium can be made by noting that D is by far the most sensitive of the various temperature dependent parameters in Equation 63. Also since this temperature is not so much above 600^{o}C we may use the 600^{o}C values of these other parameters to a reasonable approximation. As a result since this critical temperature occurs for $r^{lim} \simeq 10^{-5}$ cm the value of D required in Equation 63 is $\sim 1{\cdot}5 \times 10^{22}$ so that $T \sim 680^{o}$C.

We conclude therefore that above about 700^{o}C bubbles of all realistic sizes will be maintained approximately in equilibrium by means of the thermal equilibrium concentration of vacancies. It is difficult to conclude what quantitiative effect the irradiation produced defects have on this conclusion. However on the basis of the irradiation experiments which have resulted in void formation it seems very reasonable to assume that the radiation produced defects will not decrease the net rate at which vacancies can reach bubbles. If this rate increases, as seems quite possible, bubbles at temperature below 700^{o}C, will be able to attain equilibrium. Of course if the net arrival rate of vacancies is considerably enhanced bubbles may grow to radii much greater than r_o and so become void-like; however detailed predictions on this subject are not possible at present. (For further discussion on this point see item 4 of Section 6.2). Essentially all we can conclude with any certainty at present is that above 700^{o}C gas filled cavities will absorb at least sufficient vacancies to become, to a good approximation, equilibrium bubbles.

APPENDIX 2

Approximations to the Van der Waals Equation of State which are Permissible in Bubble Calculations

Throughout this section we shall assume that Van der Waals equation

$$\left(p + \frac{n^2 a}{V^2}\right)(V - nb) = nkT \qquad \ldots (64)$$

accurately represents the equation of state for helium at all pressures and temperatures involved in the present work, with the constants a and b equal to $9{\cdot}540 \times 10^{-38}$ dynes $cm^4/atoms^2$ and $3{\cdot}397 \times 10^{-23}$ $cm^3/atom$ respectively[5]. However deviations at high gas pressures, corresponding to small bubble radii are to be expected. Harrison[73] has recently discussed errors in the calculation of fuel element swelling due to xenon gas bubbles arising out of assuming Van der Waals equation to be the equation of state. From his conclusions and the expectation that helium will obey this particular equation of state more closely than xenon at a given temperature and pressure it seems likely that errors of not more than a few per cent are to be expected for a bubble radius of 10^{-6} cm. A more definitive statement would require a sifting of the various experimental data (e.g. see Reference 74) which for the present application would not seem to be necessary since we are mainly concerned here with bubble radii of the order 10^{-5} cm.

We shall also assume throughout this section that bubbles are in equilibrium (Equation 7) and that $T = 1000^{o}C$.

For very large bubbles, when gas pressures are low, the equation of state may be represented to a good approximation by the perfect gas law. For somewhat smaller bubbles let us assume that the equation of state can be reasonably approximated by a simplification of Equation 64:

$$p(V - nb) = nkT \; ; \qquad \ldots (65)$$

this assumption is justified below. Now one possible criterion for the perfect gas law to be a reasonable approximation of Equation 65 is

$$nb < \varphi V \qquad \ldots (66)$$

where φ is some fraction whose numerical value is less than unity. From Equations 7, 65 and 66 we find that

$$r > \frac{2\gamma b}{kT}\left(\frac{1}{\varphi} - 1\right) \qquad \ldots (67)$$

Hence for $\varphi = 0{\cdot}1$ and $0{\cdot}01$ $r > 850$ and 9300 Å respectively. As a result it seems reasonable to assume a round figure of 1000 Å as the bubble radius below which the perfect gas law is not valid.

Let us now discuss under what conditions the assumption made above, namely that the $\frac{n^2a}{V^2}$ term in Van der Waals equation may be neglected, is valid. In a manner similar to Equation 66 let us write

$$\frac{n^2a}{V^2} = \theta p \qquad \ldots (68)$$

where θ is the numerical factor less than unity which defines the limiting value below which the $\frac{n^2a}{V^2}$ term may be neglected. From Equations 64 and 68 we have therefore

$$bx^2 - x + \frac{\theta\, kT}{(1+\theta)a} = 0 \qquad \ldots (69)$$

where $x^2 = \frac{\theta p}{a}$. Solution of this quadratic in x gives two limiting values of p for the particular value of θ that is assumed between which the $\frac{n^2a}{V^2}$ term may not be neglected. The existence of both an upper and a lower limiting pressure may be appreciated by inspection of Equation 64. At very low pressures $\frac{1}{V^2}$ decreases more rapidly than p as $p \to 0$; at very high pressures $V \to nb$, so that $\frac{n^2a}{V^2}$ approaches the constant value $\frac{a}{b^2}$ as $p \to \infty$. As a result the $\frac{n^2a}{V^2}$ term may be neglected for sufficiently low and high pressures.

However a solution of Equation 69 is only possible if

$$\frac{4b\theta kT}{(1+\theta)a} \leqslant 1 \qquad \ldots (70)$$

i.e. if $\theta \leqslant 3{\cdot}4 \times 10^{-3}$. This implies that for helium $\frac{n^2a}{V^2}$ is always very small compared with p and that as a result it is always a good approximation to write Van der Waals equation in the form given in Equation 65.

In conclusion it should be noted that for many other gases it is not a good approximation to neglect the $\frac{n^2a}{V^2}$ term. We wish to make this point since in the past the $\frac{n^2a}{V^2}$ term has often been neglected without justification in the literature relating to fuel element swelling calculations.

By way of illustration let us consider xenon, for which the constants a and b are $1{\cdot}17 \times 10^{-35}$ dynes cm^4/atom^2 and $8{\cdot}48 \times 10^{-23}$ cm^3/atom respectively[5], and let us assume that the $\frac{n^2a}{V^2}$ term may be neglected if $\theta < 0{\cdot}1$. From Equation 70 there are solutions of the quadratic, Equation 69, only if $\theta \leqslant 0{\cdot}244$. For $\theta = 0{\cdot}244$, when the two roots are equal, the bubble radius corresponding to the limiting pressure is, using in addition Equation 7, 252 Å. For $\theta = 0{\cdot}1$ when there are two roots of the quadratic the corresponding limiting radii are 34 and 1450 Å. This implies that for bubble radii lying between these two limits $\theta > 0{\cdot}1$, so that the $\frac{n^2a}{V^2}$ term should be included in the Van der Waals equation in this size region.

The bubble radii corresponding to other values of θ are shown in Fig.9.

Although the $\frac{n^2a}{V^2}$ term may not be neglected over a certain size range of xenon bubbles it nevertheless affects the Van der Waals equation less than the term nb. Thus if we define ξ as $na^2/pV^2 \div nb/V$ we find that the maximum possible value of ξ is 0·79 at zero pressure, its value decreasing with increasing pressure. $\xi = 0{\cdot}1$ when $p = 1{\cdot}42 \times 10^{10}$ dynes cm^{-2}, corresponding to a bubble radius of about 29 Å.

APPENDIX 3

The Enhancement by Radiation of the Self-Diffusion

In the absence of radiation the diffusion coefficient in a pure metal, assuming a vacancy mechanism, is given by[75]

$$D = a^2\nu \exp\left[\frac{\Delta S_f + \Delta S_m}{R}\right] \cdot \exp\left[\frac{-\Delta H_f - \Delta H_m}{RT}\right] \quad \ldots (71)$$

where a is the lattice parameter, ν the atomic vibrational frequency, ΔS_f and ΔS_m the entropy changes associated with the formation and migration of a vacancy respectively and ΔH_f, ΔH_m the corresponding changes in the enthalpy. Alternatively this equation may be written as

$$D = a^2 \nu_m v_o \quad \ldots (72)$$

where ν_m is the jump rate of a vacancy and v_o the thermal vacancy concentration at temperature T. Radiation enhances the diffusion coefficient by creating an additional concentration of vacancies, v, which will be present in dynamical equilibrium. Clearly the importance of this radiation enhancement will be determined by the magnitude of v relative to v_o.

If the radiation produced defects are assumed to anneal either at sinks or by the mutual annihilation of interstitials and vacancies the steady state vacancy concentration is given by[76]

$$v = -\tfrac{1}{2}(c + v_o) + \tfrac{1}{2}\left[(c + v_o)^2 + \frac{4K}{\nu_m}\right]^{\frac{1}{2}} \quad \ldots (73)$$

where c is the sink concentration and K the point defect production rate.

During the course of the irradiation the sink concentration is expected to increase as immobile defect aggregates are formed and grow. As a result, at any instant of time, c is expected to lie somwhere within the range $10^{-5} - 10^{-2}$.

From Equations 71 and 72 v_o is approximately equal to $\exp\{-\Delta H_f/RT\}$, where for the sake of simplicity the entropy factor is put equal to unity; this should be sufficiently accurate for our present purposes. Now when diffusion is governed by a vacancy mechanism

$$Q = \Delta H_f + \Delta H_m \quad \ldots (74)$$

where Q is the activation energy for diffusion, 96·0 k.cals/mole = 4·13 eV/atom[11]. Since ΔH_m = 1·22 eV[77] ΔH_f = 2·91 eV. As a result at 600, 1000 and 1200°C $v_o = 1{\cdot}6 \times 10^{-17}$, 3×10^{-12} and $1{\cdot}1 \times 10^{-10}$ respectively.

K the point defect production rate is simply the corresponding cross section, which from Table 5 is 3010 barns, multiplied by the neutron flux. This gives the density of

Frenkel pairs produced per second as $1{\cdot}11 \times 10^{-6}$. However it is well known that the theoretical point defect production rate always exceeds those derived from experiments by approximately an order of magnitude[78]; undoubtedly one reason for this discrepancy is that many closely spaced vacancy-interstitial pairs recombine almost immediately after they are formed and so will make little contribution to the radiation enhanced diffusion. As a result we will assume K, the Frenkel pair production rate, to be 10^{-7} atomic fraction per second.

The vacancy jump rate ν_m is given by $A \exp\{-\Delta H_m/RT\}$ where A is a constant assumed here to be 10^{15} sec^{-1}[76]. Hence at 600, 1000 and 1200°C $\nu_m = 9 \times 10^7$, $1{\cdot}5 \times 10^{10}$ and 7×10^{10} jumps per second respectively.

Before applying the above numerical values to calculate v we need to justify that for times which are of interest to us the steady state vacancy concentration has been attained, so that it is permissible to use Equation 73. The build-up time, τ, required for the point defect concentration to attain saturation always lies between $\frac{1}{c\nu_m}$ and $\frac{1}{2c\nu_m}$[79,80] so that the maximum possible value of τ is $[10^{-5} \times 9 \times 10^7]^{-1} \simeq 10^{-3}$ secs. As a result for time scales which are of interest to us here we may consider that the point defect concentration saturates instantaneously at the beginning of the irradiation and Equation 73 may be used to derive the vacancy concentration.

Since $v_0 \ll c$ and $\frac{4K}{\nu_m} \ll c^2$ Equation 73 may be simplified to give

$$v = \frac{K}{\nu_m c} \qquad \ldots (75)$$

Values of v at different temperatures and for the two extreme values of c are shown in Table 8; for the sake of comparison the corresponding values of v_0 are also shown.

TABLE 8

Values of v, the radiation-induced steady state vacancy concentration and v_0 the thermal equilibrium concentration

Temperature °C \ Impurity Concentration	10^{-5}	10^{-2}	v_0
600	$1{\cdot}1 \times 10^{-10}$	$1{\cdot}1 \times 10^{-13}$	$1{\cdot}6 \times 10^{-17}$
1000	7×10^{-13}	7×10^{-16}	3×10^{-12}
1200	$1{\cdot}4 \times 10^{-13}$	$1{\cdot}4 \times 10^{-16}$	$1{\cdot}1 \times 10^{-10}$

From Table 8 it is evident that at 1000 and 1200°C v is appreciably smaller than v_o so that over this temperature range radiation does not enhance the diffusion coefficient significantly. At 600°C however $v \gg v_o$ so that the enhancement of the diffusion by radiation is now appreciable. In this case the overall diffusion coefficient is given to a good approximation by Equation 72 with v_o replaced by v. If we put $v = 5 \times 10^{-12}$, a figure which lies about half way between the two values given in Table 8 we find that $D = 5 \times 10^{-19}$ cm^{-2} sec^{-1}.

The above discussion assumes that diffusion occurs by the migration of vacancies, an assumption which from our present state of knowledge seems reasonably justified. The self diffusion coefficient has been employed on two occasions in this work: (a) In Section 3.2.2.1 to describe the migration of helium atoms to bubbles. On the basis of calculations[22] and experimental evidence[81,82] it seems reasonable to assume that helium atoms are located substitutionally in the lattice and are attached to one or two vacancies (see also Section 3.2.4). (b) The growth of gas filled cavities to form bubbles which are approximately in equilibrium (Appendix 1). While the possibility that these processes may occur by an interstitial or some other mechanism cannot be completely ruled out a vacancy mechanism seems conceptually more understandable and reasonable.

If in fact interstitials do play a part in diffusion we note that their contribution is identical in magnitude to that due to radiation produced vacancies since it may be shown that $\nu_m v = \nu_m' i$, where i and ν_m' are respectively the concentration and jump rate of interstitials. In comparison diffusion due to thermally produced interstitials is negligible since the equilibrium concentration is always much smaller than i.

It is interesting to note that when diffusion is dominated by the radiation produced defects there are certain conditions for which the diffusion coefficient is independent of temperature. From Equations 72 (with v_o replaced by v) and 75 we have

$$D = \frac{a^2 K}{c} \qquad \ldots (76)$$

which is temperature independent provided that the assumptions made in deriving Equation 75, namely $v_o \ll c$ and $\frac{4K}{\nu_m} \ll c^2$, are valid. For situations of interest here the first of these conditions is always valid. The second requires that $\nu_m > 4 \times 10^3$ and 4×10^{-3} for c values of 10^{-5} and 10^{-2} respectively. This implies that the respective temperatures of the specimen should be greater than about 270 and 80°C. Note however that if, as seems likely, c is time dependent D wil be also. Clearly therefore for the lower range of possible temperatures at which the containment vessel may be operated the diffusion will be temperature independent, at least for one instant in time. As a result in this temperature

region the nucleation and growth of bubbles and also their ability to attain equilibrium will be little affected by temperature fluctuations of the containment vessel.

It will be noted that in Section 3.2 no attempt was made to allow for the effect of radiation on the surface and grain boundary diffusion coefficients. This is because such allowance is very difficult in view of our lack of understanding of the detailed atomic mechanisms.

APPENDIX 4

The Predominant Mechanism by which Bubbles Migrate

Conceivably there are three possible ways by which bubbles can move. (a) Surface diffusion: Niobium atoms on the bubble-solid interface migrate along the surface of the bubble. (b) Volume diffusion: Niobium atoms on the surface of the bubble migrate to another point on the surface by diffusion along a path which lies within the solid. (c) Evaporation: Niobium atoms evaporate into the bubble and subsequently condense at another point on the surface. We shall now demonstrate that surface diffusion is the most important of these three mechanisms.

The velocity of a bubble under the action of a driving force $\underset{\sim}{F}$ is given by the Einstein relationship

$$\underset{\sim}{V} = \frac{A}{kT}\underset{\sim}{F} \qquad \ldots (77)$$

where A is some diffusion coefficient whose value is determined by the various mechanisms which are operating. For mechanisms (a) (b) and (c) above we shall write the corresponding components of this coefficient as A_S, A_V and A_E respectively. It can be shown that[17]

$$A_S = \frac{3D_S\Omega^{4/3}}{2\pi r^4} \qquad \ldots (78)$$

where D_S is the surface diffusion coefficient, Ω the atomic volume and r the bubble radius. A_V is given by[83]

$$A_V = \frac{\Omega D_V}{\pi r^3} \qquad \ldots (79)$$

where D_V is the volume diffusion coefficient. The corresponding expression for A_E is[17]

$$A_E = \frac{9\Omega^2 P_V}{64\pi r^2 \sigma^2 \gamma}\left(\frac{M_{He} + M_{Nb}}{M_{He}\,M_{Nb}} \cdot \frac{RT}{2\pi}\right)^{1/2} \qquad \ldots (80)$$

where P_V is the vapour pressure of niobium in bubbles, σ the cross sectional radius for collisions between helium and niobium atoms, γ the surface energy per unit area and M_{He}, M_{Nb} the masses in atomic mass units of helium and niobium.

In order to assess the importance of volume diffusion compared with surface diffusion consider the ratio

$$\frac{A_S}{A_V} = \frac{\Omega^{1/2}}{r}\frac{D_S}{D_V} . \qquad \ldots (81)$$

With $D_S = 1{\cdot}3 \times 10^{-16}$, 10^{-11} and $4{\cdot}1 \times 10^{-10}$ cm^{-2} sec^{-1} at 600 and 1000 and 1200°C respectively and with corresponding values for D_V of 5×10^{-19}, $4{\cdot}7 \times 10^{-17}$ and $7{\cdot}6 \times 10^{-15}$ cm^{-2} sec^{-1} we find that $A_S > A_V$ provided that $r < 7 \times 10^{-6}$, 5×10^{-3} and

10^{-3} cm respectively. At 1000 and 1200°C it is evident therefore that for bubbles of sizes which are of interest to us here surface diffusion is more important than volume diffusion. The reason why an appreciably different critical radius has been obtained at 600°C compared with the other two temperatures is because a radiation-enhanced value for D_V but not for D_S was used (Appendix 3). This is probably an unrealistic assumption since if D_V is enhanced by radiation it is likely, if surface diffusion involves vacancy migration, that D_S will be also. As a result the critical radius would be expected to be larger than 7×10^{-6} cm. We conclude therefore that apart from some reservations for temperatures around 600°C surface diffusion will always be a more important mechanism than volume diffusion.

In order to assess the importance of evaporation relative to surface diffusion values of A_S and A_E were calculated at temperatures of 600, 1000 and 1200°C; the results are shown in Table 9. The following values of the various parameters were assumed: $r = 10^{-5}$ cm, $P_V = 6 \times 10^{-38}$, 4×10^{-19} and 5×10^{-15} mm at 600, 1000 and 1200°C[11], $\sigma = 2 \times 10^{-8}$ cm[5].

TABLE 9

A comparison between the constants A_S and A_E, relating respectively to the migration of bubbles by surface diffusion and evaporation

Temperature °C	A_S	A_E
	$cm^{-2}\ sec^{-1}$	
600	3×10^{-27}	8×10^{-54}
1000	2×10^{-22}	5×10^{-35}
1200	9×10^{-21}	9×10^{-31}

It is apparent that $A_S \gg A_E$ at all temperatures so that evaporation is a comparatively unimportant mechanism by which bubbles migrate. Although this result was derived from a bubble radius of 10^{-5} cm it may be readily shown, from a consideration of Equations 78 and 80, to be valid for all realistic bubble sizes. However owing to the rapid increase in A_E with temperature evaporation will be the most important mechanism for bubble migration at temperatures closer than those considered here to the melting point.

Reference 83 gives a more general discussion of the relative importance of the three migration mechanisms as a function of temperature and bubble radius.

We conclude therefore that for temperatures and bubble sizes which are of interest here it is permissible to assume that bubble migration occurs entirely as a result of niobium atoms diffusing along the gas/solid interface.

REFERENCES

1. CARRUTHERS, DAVENPORT and MITCHELL. Culham Laboratory Report CLM-R 85 (1967).

2. ROSE. Oak Ridge National Laboratory Report ORNL-TM-2204 (1968).

3. HOMEYER. Massachusetts Institute of Technology Report MIT-TR-435 (1965).

4. STEHN, GOLDBERG, MAGURNO and WEINER-CHASMAN. Brookhaven National Laboratory Report BNL, 325, 2nd edition, supplement II, (1964).

5. Handbook of Chemistry and Physics, 48th Edition, 1967-8, (Chemical Rubber Co., Cleveland).

6. KINCHIN and PEASE. Rept. Prog. Phys. 18, 1 (1955).

7. ELLIOTT. Constitution of Binary Alloys, 1st Supplement. (McGraw Hill, New York, 1965).

8. FESCHOTTE, LIVEY and Von GOLDBECK, Atomic Energy Review, Special Issue No.2, 45 (1968).

9. SISCO and EPREMIAM. Columbium and Tantalum, p.255 ff. (Wiley, New York, 1963).

10. GREGORY and ROWE. Columbium Metallurgy, edited by Douglass and Kunz, p.309. (Interscience, New York, 1961).

11. SMITHELS. Metals Reference Book, 4th edition. (Butterworths, London, 1967).

12. WEBB. Atomics International, Calif., Report NAA-SR-10462 (1965).

13. INMAN and TIPPLER. Met Rev. 8, 121 (1963).

14. BARNES. Harwell Report AERE-R.4429 (1963).

15. GREENWOOD, FOREMAN and RIMMER. J. Nucl. Mat. 1, 305 (1959).

16. GREENWOOD, and SPEIGHT. J. Nucl. Mat. 10, 140 (1963).

17. NICHOLS, U.S.A.E.C. Report, WAPD-TM-570 (1966).

18. MARTIN. J. Nucl. Mat. 33, 23 (1969); also Harwell Report AERE-R.6024 (1969).

19. TIMOSHENKO and GOODIER. Theory of Elasticity, 2nd edition, p.412. (New York, McGraw Hill, 1951).

20. CHATWIN and HYAM. U.K.A.E.A. Reactor Group, Windscale Report, TRG Rep. 325(W) (1962).

21. LOMER. Progress in Metal Physics 8, 255 (1969).

22. RIMMER and COTTRELL. Phil. Mag. 2, 1345 (1957).

23. LANG. Summer School on "Recent Developments in Diffraction Techniques Applied to Materials Science". (1969). To be published by North Holland.

24. NELSON. Cockcroft-Libby Conference, (September 1968).

25. TURNBULL. C.E.G.B., Berkeley Nuclear Laboratories, Report RD/B/N.1112 (1968).

26. Columbium Metallurgy, edited by Douglass and Kunz (Interscience, New York, 1961).

27. ODETTE. Thesis M.I.T. Department of Nuclear Engineering (January 1968).

28. WESTERN, WILLIAMS, and CARTER. Conference on Neutron Cross-Section Technology, 22-24 March, 1966, Washington, (CONF.660303, p.675).

29. Brookhaven National Laboratory report BNL 400.

30. HYDER and KENWARD. Harwell Report AERE-R.2886. (1959).

31. THOMSON. Phys. Rev. 129, 1649 (1963).

32. LUCASSON and WALKER. Phys. Rev. 127, 485 (1962).

33. LINDHARD, NIELSEN, SCHARFF and THOMSEN. Kgl. Danske Videnskab. Selskab, Mat.-Fys. Medd. 33, No.10 (1963).

34. MYERS. Conference on Nuclear Fusion Reactors, paper 4.4, Culham (1969).

35. SEITZ and KOEHLER. Solid State Physics, 2, 425 (1956).

36. ROBINSON. Conference on Nuclear Fusion Reactors, paper 4.3, Culham (1969).

37. MAKIN and MINTER. Acta Met. 7, 361 (1959).

38. EVANS, WEINBERG and Van THYNE. Acta Met. 11, 143 (1963).

39. OHR, TUCKER and BOLLING. Oak Ridge National Laboratory Reports ORNL 4246 and 4250 (1968).

40. KANGILASKI. Reactor Materials 11, 176 (1968)

41. MOTEFF. Radiation Effects p.727 (Gordon and Breach, New York, 1967).

42. HOLMES, ROBBINS, BRIMHALL and MASTELL. Acta Met. 16, 955 (1968).

43. WIFFEN and STIEGLER. Battelle-Northwest, Richland, Wash., report BNWL-870, p.11.79 (1968).

44. HARKNESS. Battelle-Northwest, Richland, Wash., report BNWL-870, p.3.4 (1968).

45. BRIMALL and MASTELL. J. Nucl. Mat. 29, 123 (1969).

46. MASTEL and BRIMHALL. J. Nucl. Mat. 28, 115 (1968).

47. STIEGLER, FARREL, DuBOSE and KING. I.A.E.A. Symposium on Radiation Damage in Reactor Materials. Paper SM-120/F-5 (1969).

48. KING and LONG. J. Metals 20, No.8, 116A (1968).

49. CAWTHORNE and FULTON. Nature 216, 575 (1967).

50. NELSON and MAZEY. I.A.E.A. Symposium on Radiation Damage in Reactor Materials. Paper SM-120/F-1 (1969).

51. HOLMES and BRAGER. Trans. Amer. Nucl. Soc. 11, 479 (1968).

52. HONEYCOMBE. The Plastic Deformation of Metals, p.352 (Arnold, (1968)).

53. TOTTLE. Nucl. Eng. 3, 212 (1958).

54. BEGLEY. Wright Air Development Center, Ohio Report WADC-TR-57-344 (1957).

55. See Reference 10.

56. BRINSON and ARGENT. J. Inst. Metals 91, 293 (1963).

57. RAWSON and ARGENT. J. Inst. Metals 95, 212 (1967).

58. SHOEK. J. Appl. Phys. 29, 112 (1958).

59. MOSEDALE. J. Appl. Phys. 33, 3142 (1962).

60. HESKETH. J. Nucl. Mat. 29 77 (1969).

61. BUCKLEY. Harwell Report AERE-R.5944, p.547 (1968).

62. BILLINGTON and CRAWFORD. Radiation Damage in Solids (Princeton University Press, 1961).

63. LUSTMAN and KERZE. The Metallurgy of Zirconium. (McGraw Hill, New York, 1955).

64. ENGE. Introduction to Nuclear Physics. (Addison-Wesley, (1966)).

65. KELLER. Harwell Report AERE-R.5464 (1967).

66. ALMEN and BRUCE. Nucl. Inst. and Methods 11, 257 (1961).

67. GARBER, DOLYA, KOLYADA, MODLIN and FEDERENKO. J.E.T.P. Letters 7, 296 (1968).

68. THOMPSON and NELSON. Phil. Mag. 7, 2015 (1962).

69. NELSON and SHELDON. Phil. Mag. 11, 291 (1965).

70. BLOW, CROCKER and WADE. Conference on Nuclear Fusion Reactors, paper 5.5, Culham (1969).

71. STEINER. Conference on Nuclear Fusion Reactors, paper 5.4, Culham (1969).

72. LIDSKY and COLOMBANT. Massachusetts Institute of Technology, Research Laboratory of Electronics, Progress Report (January 1968).

73. HARRISON. J. Nucl. Mat. 31, 99 (1969).

74. KEESOM. Helium (Elsevier, Amsterdam, 1942).

75. SHEWMON. Diffusion in Solids (McGraw Hill, New York, 1963).

76. DIENES and DAMASK. J. Appl. Phys. 29, 1713 (1958).

77. PEACOCK and JOHNSON. Nature 195, 169 (1962).

78. HOLMES. The Interaction of Radiation with Solids, edited by R. Strumane et al. (North Holland, Amsterdam, (1964)).

79. LOMER. Harwell Report AERE T/P 1540 (1954).

80. SHARP and FOREMAN. Harwell Report AERE-R.5786 (1968).

81. RUSSEL and HASTINGS. J. Nucl. Mat. 17, 30 (1965).

82. VELA, HARDY and RUSSEL. J. Nucl. Mat. 26, 129 (1968).

83. BARNES and NELSON. Harwell Report AERE-R.4952 (1965).

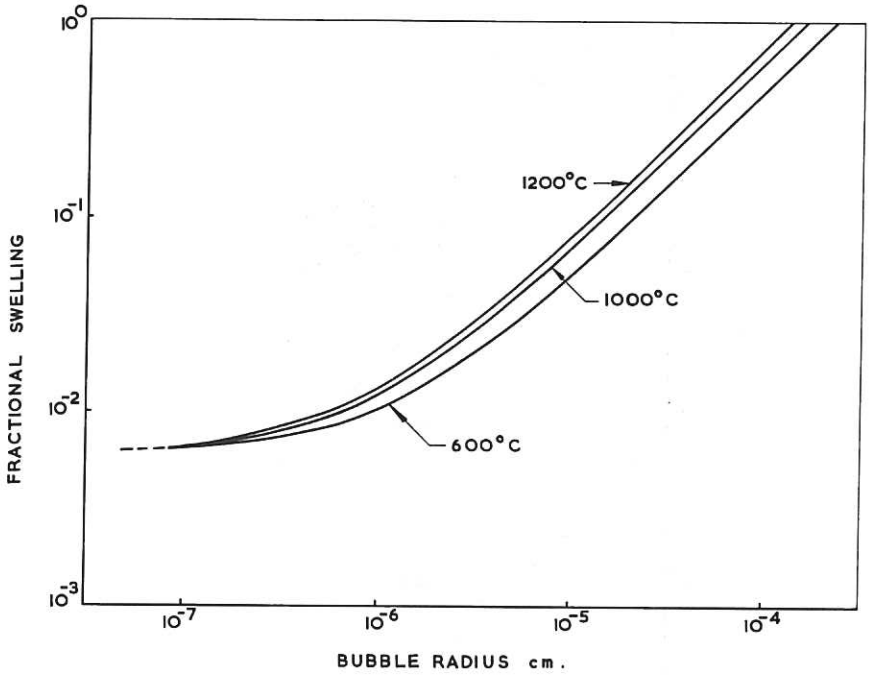

Fig.1 The fractional swelling of niobium as a function of bubble radius.

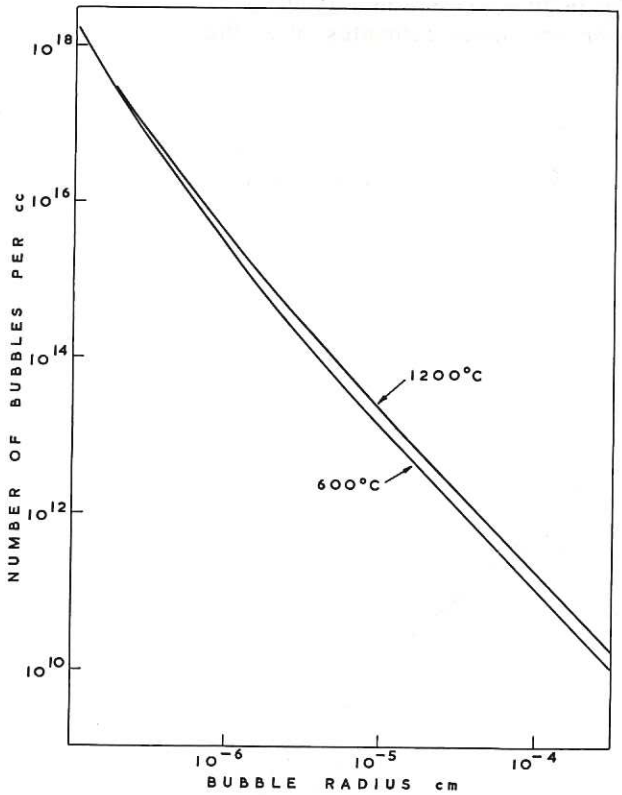

Fig.2 The number of bubbles per cc as a function of bubble radius.

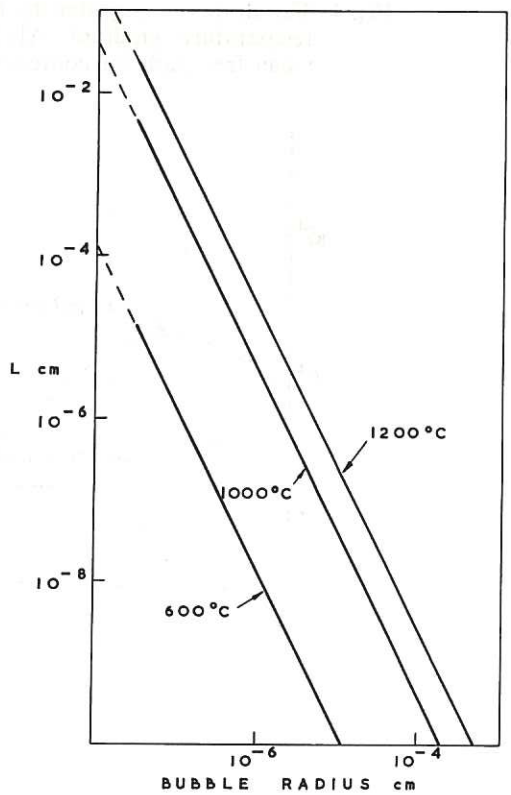

Fig.3 The distance migrated by bubbles in 20 years due to Brownian motion.

CLM-R 103

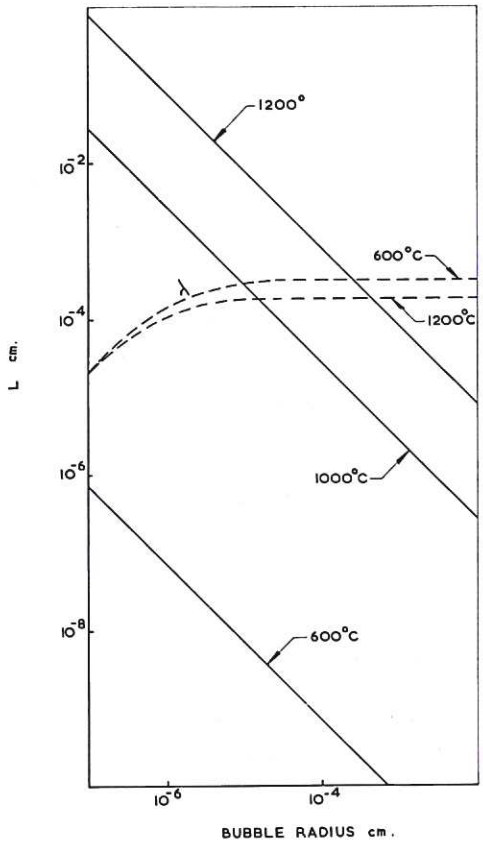

Fig.4 The distance migrated by bubbles in 20 years due to a 250°C cm^{-1} temperature gradient. Also shown are upper estimates of λ the mean free path for coalescence.

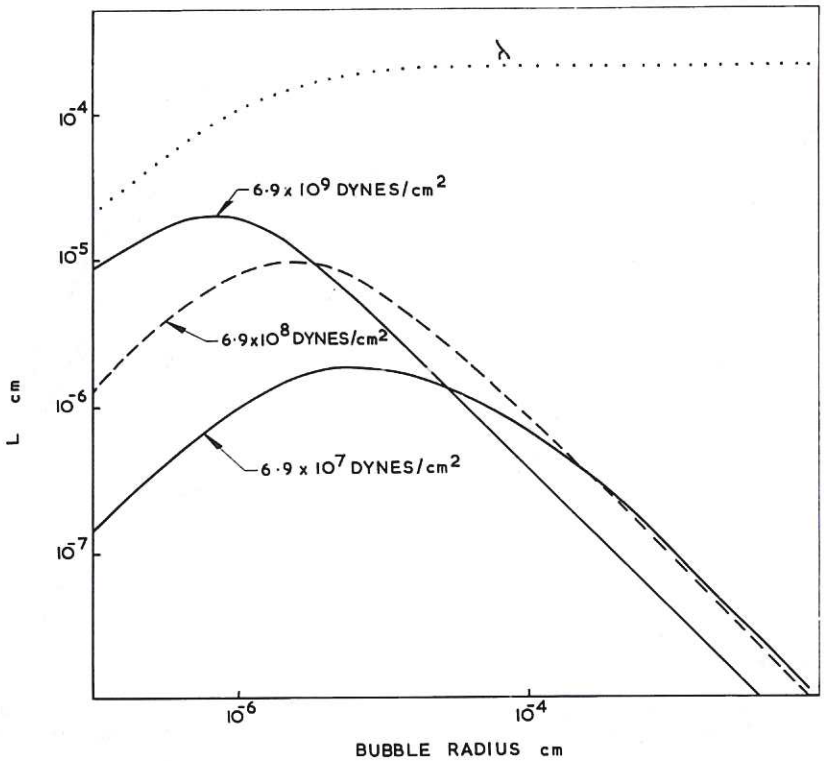

Fig.5 The distance migrated by bubbles at 1000°C in 20 years for various compressive stresses and in a stress gradient of 3×10^{9} dynes cm^{-3}. As in Fig.4 an upper estimate of the mean free path for coalescence is also shown.

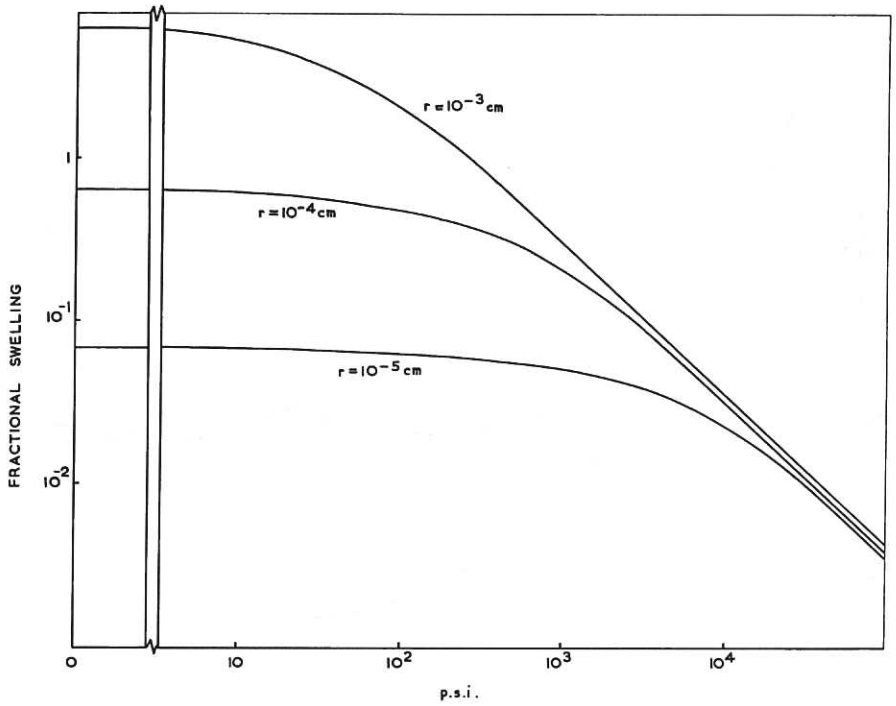

Fig.6 The reduction in the swelling of niobium by the application of a hydrostatic compressive stress. Values of the bubble radius shown apply for when the stress is zero.

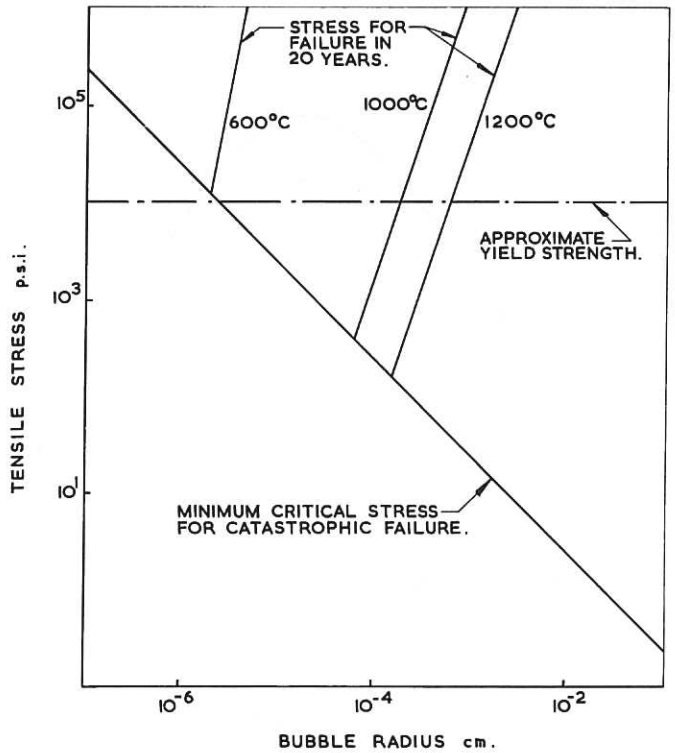

Fig.7 σ_{crit}, the tensile stress above which bubbles cannot maintain equilibrium, and the stress at three temperatures for fracture to occur after 20 years.

CLM-R103

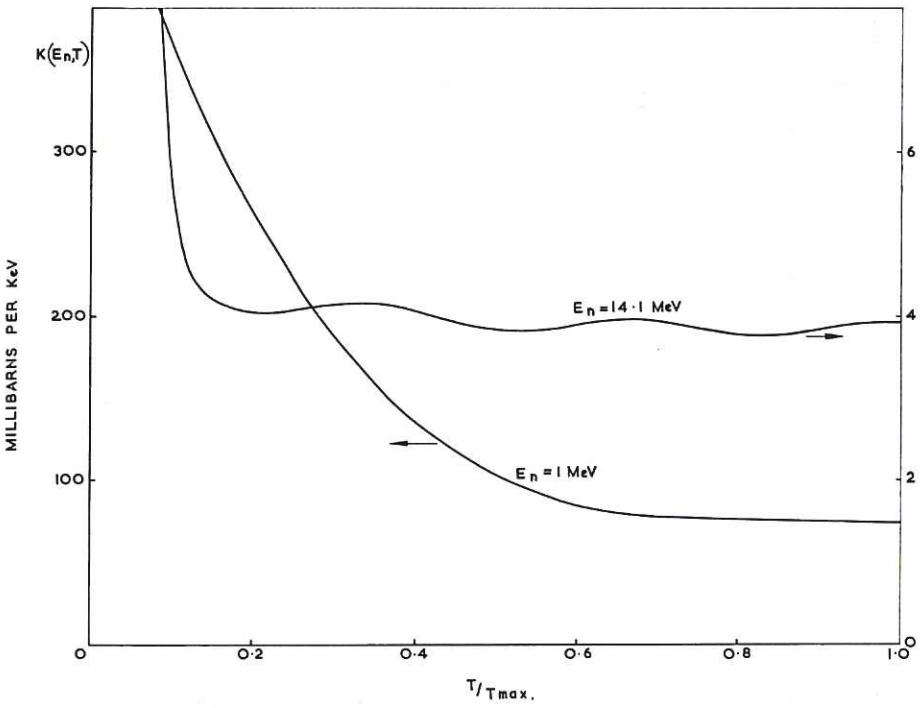

Fig.8 The cross section for transferring energy T to a lattice atom by a neutron of energy E_n.

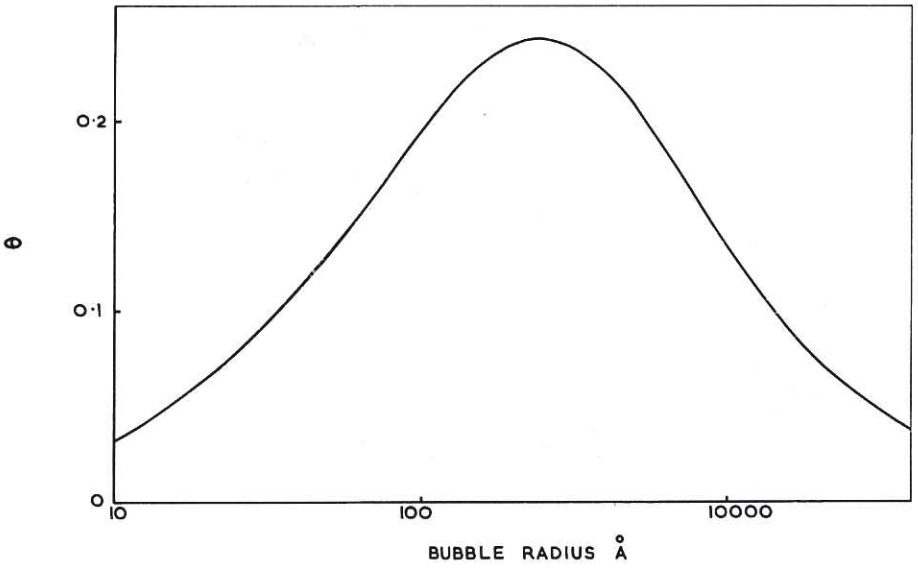

Fig.9 The importance of the $\frac{n^2a}{V^2}$ term in the Van der Waals equation as a function of radius for a xenon bubble. CLM-R103

Available from

HER MAJESTY'S STATIONERY OFFICE

49 High Holborn, London, W.C.1
13a Castle Street, Edinburgh 2
109 St. Mary Street, Cardiff CF1 1JW
Brazennose Street, Manchester M60 8AS
50 Fairfax Street, Bristol BS1 3DE
258 Broad Street, Birmingham 1
7-11 Linenhall Street, Belfast BT2 8AY

or through any bookseller.